Analysis Of The XY Spin 1/2 Model In Staggered Field And Networks Of D-Wave Josephson Junctions

Richard Henry Crooks

A dissertation submitted to the faculty of the University of North Carolina at Chapel Hill in partial fulfillment of the requirements for the degree of Doctor of Philosophy in the Department of Physics & Astronomy.

Chapel Hill
2012

Approved by:

Dmitri Khveshchenko

Jon Engel

Charles Evans

Sean Washburn

Yueh Wu

ABSTRACT

Richard Henry Crooks: Analysis Of The XY Spin 1/2 Model In Staggered Field And Networks Of D-Wave Josephson Junctions
(Under the Direction of Dmitri Khveshchenko)

The study of entanglement in quantum systems is an area of much recent experimental and theoretical work and is of central importance in the implementation of various protocols in quantum information science. The dynamical properties of entanglement are examined in the context of the XY spin 1/2 chain model with a staggered magnetic field. The quality of entangled state transfer is found to be comparable to the uniform field XY spin 1/2 chain in the strong field regime. The effects of anisotropy on state transfer is also considered, as well as the interaction between entanglement waves and the possibility of transmission of multiple bits of quantum information.

As an additional system where these quantum entanglement dynamics might play out, a large array of mesoscopic junctions made out of gapless unconventional superconductors is also studied. In this model, the tunneling processes of both particle-hole and Cooper pairs give rise to a strongly retarded effective action which, contrary to the case of conventional superconductors, cannot be readily characterized in terms of a local Josephson energy. This is an action that describes, for example, grain boundary and c-axis junctions in layered high-T_c superconductors. The emergent collective phenomena in this system are obtained, along with the phase diagram and the electrical conductivity of the model.

To my mother, Audrey

ACKNOWLEDGMENTS

I would like to thank my advisor Dr. Dmitri Khveshchenko for his constant support and guidance. Also thanks to the entire faculty and staff of the Department of Physics and Astronomy of the University of North Carolina at Chapel Hill for an excellent graduate education. Lastly, I thank my family and friends for their love and support.

Richard Henry Crooks

April 29, 2012

CONTENTS

LIST OF FIGURES

Chapter 1

Introduction

Quantum systems possess a type of correlation, called entanglement, that has no analogue in a classical system [1]. This property of quantum states was realized early on [2, 3] and is central to the discussion of the nature of quantum mechanics. More recently, the study of entanglement has centered on its role in the study of quantum phase transitions [4] as well as quantum information theory[5]. Long range correlations arise in the vicinity of a quantum phase transition, and the emergent entanglement is an indication of the critical thermodynamical behavior of the system. On the other hand, quantum information theory treats entanglement as a resource that is necessary for the implementation of various quantum information protocols, including superdense coding[6], quantum teleportation[7] and quantum computation[8, 5].

A successful physical implementation of these quantum computing protocols hinges on the ability to generate, detect, and achieve a high fidelity transfer of entangled quantum states in some physical system. A number of experimental efforts have attempted to address these needs, including work in photonic [9], cavity QED[10], quantum dot[11], and atomic systems[12], as well as mesoscopic devices such as Josephson junctions[13, 14, 15]. Over long distances, the ideal mode of transport of an entangled state is via quantum teleportation using entangled photons in an optical fiber. For much shorter distances, such as the distances between the various components (core processor, storage, etc.) of a quantum register, it is preferable to employ a communication channel that is directly coupled to these components.

Specifically, recent proposals have focused on the use of one-dimensional chains of permanently coupled spin 1/2-like variables of stationary qubits whose practical implementation might be possible with cold atoms in optical lattices, Josephson junction and quantum dot arrays, or other two-level systems. As a salient feature of any periodic array, the translational invariance of the chain facilitates the emergence of quantum states with definite momentum, thereby enabling a high-fidelity spatial transfer of entanglement.

Spin 1/2 chains are the preferred context in which to study entanglement transfer because of applicability of the Bethe ansatz [16] and other techniques to a wide range of models. Studies have considered spin 1/2 chains with ferromagnetic [17, 18, 19], antiferromagnetic [20], short and long-range, and SU2- versus U1-invariant exchange couplings. On the other hand, much less attention has been paid to different patterns of the local field, almost all the studies being conducted in, from a technical standpoint, the simplest case of a spatially uniform field. Considering, however, that a local field can be used for both initialization and readout of a quantum register, a comprehensive analysis of different local field distributions is strongly warranted. The main thrust of Chapter 3 is to put forth a spin 1/2 model with a spatially nonuniform field and compare its entanglement dynamics it with the previously discussed uniform field case[21, 22].

Before doing this, however, a review of some of the technical aspects of quantum entanglement is required. In Chapter 2 some notions in the field of quantum information science are introduced, including relevant definitions, ways to measure entanglement, and also methods for calculating these measures. This is presented using density matrix formalism along with a general method to calculate the matrix elements for two-level fermionic systems. In Chapter 3 these methods are applied to the problem of uniform and staggered field spin 1/2 models.

Another system exhibiting collective mode phenomena is studied in Chapter 4, that of networks of Josephson junctions. A method for determining the phase diagram of a network of two-dimensional unconventional (d-wave) superconductors is presented, along with a calculation of its electrical conductivity characteristics. Most of the pre-

vious theoretical studies are limited to the Josephson junctions between conventional, fully gapped, s-wave superconductors[23].

Although the case of the d-wave superconducting cuprates, such as biepitaxial grain boundary(in-plane) Josephson junctions in Yttrium Barium Copper Oxide (YBCO) or intrinsic c-axis (vertical) ones in $Bi_2Sr_2Ca_{n-1}Cu_nO_{2n+4+x}$ with n=2, or Bi2212, has been rather extensively studied as well[24, 25, 26, 27], all such analyses would routinely resort to a phenomenological description similar to that of the gapped (s-wave) superconductors. In contrast, a microscopic analysis of a single d-wave Josephson junction [28, 29, 30] shows that the processes of both particle-hole and Cooper pair tunneling can give rise to equally nonlocal (in the time domain) terms in the effective action, thereby invalidating the very notion of a local Josephson energy. In Chapter 4, the solution for the phase diagram and electrical conductivity takes into account the microscopically justified as opposed to the phenomenological description of the unconventional Josephson junctions, by retaining the nonlocal Josephson terms in the action.

The final chapter summarizes the ideas put forward in this work as well and serves introduction to some of the recent developments in the field of entanglement dynamics.

Chapter 2

Overview Of Quantum Entanglement

A fundamental difference between systems of classical and quantum systems is that whereas the state of a system of classical objects may be uniquely specified, in a quantum system the objects may exist in a superposition of the allowable states. Each object in a classical system has a unique set of coordinates that determine its state. This cannot be said for a system of quantum particles, where a particle may be in a state that depends essentially upon the state of one or more other particles in the system. It is this notion of entangled particles that is the fundamental concern of the field of quantum information processing, which addresses problems ranging from philosophical questions about the nature of quantum mechanics to applications in emergent technologies such as quantum computation.

This chapter is not meant to be an exhaustive survey of quantum information science, instead it will serve to introduce some of the concepts about entanglement that will be used in subsequent chapters. This overview will include definitions, methods for quantifying the degree of entanglement present in a system, and examples related to entangled systems specific to two-level systems, and a brief survey of models where these notions of entanglement are commonly studied.

2.1 Definitions

Consider a quantum system composed of two sub-systems A and B of dimension m and n respectively, along with their associated Hilbert spaces $H_A^{(m)}$ and $H_B^{(n)}$ with bases $\{|\alpha_i\rangle\}_{i=1}^m$ and $\{|\beta_j\rangle\}_{j=1}^n$. The Hilbert space of the *bi-partite* system $H_A \otimes H_B$ is spanned by $\{\{|\alpha_i\rangle\} \otimes \{|\beta_j\rangle\}\}_{i=1,j=1}^{m,n}$ and the bi-partite quantum state $|\psi\rangle$ representing the system has the form

$$|\psi\rangle = \sum_{i=1}^{m} \sum_{j=1}^{n} c_{ij} |\alpha_i\rangle \otimes |\beta_j\rangle . \tag{2.1}$$

If c_{ij} may be written as $a_i b_j$ for all i and j then it is possible to write

$$|\psi\rangle = \sum_{i=1}^{m} a_i |\alpha_i\rangle \otimes \sum_{j=1}^{n} b_j |\beta_j\rangle = |\psi_1\rangle \otimes |\psi_2\rangle . \tag{2.2}$$

In this case $|\psi\rangle$ is a *separable* state, having the consequence that local operations performed on one of the subsystems do not affect the state of the other system.

This general expression Eq. 2.1 can be simplified through the use of the Schmidt Decomposition, which makes it possible to find new bases $\{|\alpha_i'\rangle\}_{i=1}^m$ and $\left\{\left|\beta_j'\right\rangle\right\}_{j=1}^n$ for H_A and H_B and coefficients $\{c_i\}$ so that the state $|\psi\rangle$ in equation 2.1 takes the form

$$|\psi\rangle = \sum_{i=1}^{Min(m,n)} c_i |\alpha_i\rangle \otimes |\beta_i\rangle , \tag{2.3}$$

where in the above equation the primes have been omitted.

2.1.1 Bi-Partite States

An important example which will appear in the rest of this work is the bi-partite state where systems A and B each represent a two-level system. Typically this is imagined as a spin 1/2 particle in a magnetic field taken to be in the $+\hat{z}$ direction, but could just as well be any other system with two relatively isolated energy levels such as a quantum dot, Josephson junction, etc. Using the notation for the usual S^z diagonal basis for the spin system the bases for A and B are $\{|\alpha_i\rangle\}_{i=1}^m = \{|\beta_j\rangle\}_{j=1}^n = \{|\uparrow\rangle, |\downarrow\rangle\}$, and the basis that spans the composite system $A \otimes B$ is the set of separable

states $\{|\uparrow\rangle_A \otimes |\uparrow\rangle_B, |\downarrow\rangle_A \otimes |\downarrow\rangle_B, |\uparrow\rangle_A \otimes |\downarrow\rangle_B, |\downarrow\rangle_A \otimes |\uparrow\rangle_B\}$. This notation is needlessly cumbersome and the conventional way to write these bi-partite forms is to drop the subscripts and multiplication and instead write, for example $|\uparrow\rangle_A \otimes |\downarrow\rangle_B \rightarrow |\uparrow\downarrow\rangle$.

The bi-partite system, of course, may be in a superposition of these basis states. Four states, which happen to be orthogonal and thus also form a basis for the bi-partite two level system, are the Bell States after John S.Bell[3][1]

$$\begin{aligned}
\left|\psi^-\right\rangle &= \frac{1}{\sqrt{2}}\left(|\uparrow\downarrow\rangle - |\downarrow\uparrow\rangle\right) \\
\left|\psi^+\right\rangle &= \frac{1}{\sqrt{2}}\left(|\uparrow\downarrow\rangle + |\downarrow\uparrow\rangle\right) \\
\left|\phi^-\right\rangle &= \frac{1}{\sqrt{2}}\left(|\uparrow\uparrow\rangle - |\downarrow\downarrow\rangle\right) \\
\left|\phi^+\right\rangle &= \frac{1}{\sqrt{2}}\left(|\downarrow\downarrow\rangle + |\uparrow\uparrow\rangle\right).
\end{aligned} \tag{2.4}$$

The first of these states, $|\psi^-\rangle$, is the spin *singlet* state for which the total spin $\left\langle \mathbf{S}^2 \right\rangle = 0$. The remaining three, $|\psi^+\rangle$, $|\phi^-\rangle$, and $|\phi^+\rangle$ each have $\left\langle \mathbf{S}^2 \right\rangle = 1$ and are called the spin *triplet* states. An important property of each of these states is that they are not separable. If a observer measures $\langle\psi^+| S_A^z |\psi^+\rangle$ the result will $+1/2$ or $-1/2$ with equal probabilities. However if a subsequent observer measures S_B^z, the result is completely determined by what the result of the measurement of the spin in subspace A. If A is measured to be $+1/2$ then B will be $-1/2$, and similarly if A is $-1/2$ then B will be $+1/2$. This phenomena where the properties of different subspaces have a similar inter-dependent relation is called *quantum entanglement*, and quantum states that exhibit this property are said to be *entangled* states.

For some time the problem of entangled states posed a challenge to the theory of quantum mechanics[2]. The essential argument is that if two particles are prepared in one of the Bell states and are allowed to propagate away from each other, forming a so-called Einstein-Podolsky-Rosen (EPR) pair, then a subsequent measurement made on one of the particles would instantaneously determine the state of the other particle, resulting in an apparent violation of local realism. Bell[3] showed that this is not generally the case, and subsequent experiments are in agreement[31]. The essential result

is that while a measurement on particle A does instantaneously determine particle B's state, no information can be transferred this way.

2.1.2 Mixed States And The Reduced Density Matrix

As previously mentioned the composite system $H_A \otimes H_B$ may be represented by the bi-partite state 2.3. This is a *pure* state, as it represents a single vector in the composite Hilbert space $H_A \otimes H_B$. On the other hand, only if $|\psi(t)\rangle$ happens to be separable can the system represented by H_A be assigned pure quantum state. If the Hamiltonian operating on $H_A \otimes H_B$ contains interactions between elements of the two subspaces, which is the case of the models considered in this work, even an initially separable state will acquire non-separable contributions. As a consequence, it is not possible to assign a pure state to only one of the component systems. In this case, the states representing each subsystem are said to be *mixed*, and are represented by a density matrix.

The density matrix representing the composite system is

$$\rho = |\psi\rangle \langle\psi| = \sum_i \sum_j c_i c_j^\star |\alpha_i\rangle \otimes |\beta_i\rangle \langle\beta_j| \otimes \langle\alpha_j| . \tag{2.5}$$

The *reduced* density matrix ρ_A, representing the mixed state of A is defined as the result of the partial trace over the elements of H_B

$$\rho_A = \mathrm{Tr}_B(\rho) = \sum_i c_i^2 |\alpha_i\rangle \langle\alpha_i| . \tag{2.6}$$

The density matrix is diagonal because $\{\alpha_i\}$ and $\{\beta_i\}$ are the bases found through the Schmidt decomposition. In practice it may not be possible to find the Schmidt basis prior to computing the reduced density matrix, but for reduced density matrices with small rank the diagonal basis is easily found once the density matrix in some other basis is known.

The mixed state represented by ρ_a is reminiscent of a classical probability distribution $p_1, p_2, \ldots, p_m$, whos entropy is known to be given by the Shannon entropy

[32],

$$S_S = -\sum_i p_i \log_2(p_i). \tag{2.7}$$

Formally, since ρ_A is not a classical probability distribution, but a probability over an ensemble, the associated entropy is given by the Von Neumann entropy,

$$S = \mathrm{Tr}(\rho_A \log_2 \rho_A). \tag{2.8}$$

This definition of the Von Neumann entropy allows the calculation of the entropy of each Bell states in the previous section, which all have $S = 1$. Any other state, for example the pure state

$$|\psi_{\alpha,\beta}\rangle = \frac{1}{\sqrt{\alpha^2 + \beta^2}} \left(\alpha \,|\uparrow\downarrow\rangle + \beta \,|\downarrow\uparrow\rangle\right) \tag{2.9}$$

has entropy

$$S = -\sqrt{\frac{\alpha^2}{\alpha^2+\beta^2}} \log_2 \sqrt{\frac{\alpha^2}{\alpha^2+\beta^2}} - \sqrt{\frac{\beta^2}{\alpha^2+\beta^2}} \log_2 \sqrt{\frac{\beta^2}{\alpha^2+\beta^2}}. \tag{2.10}$$

This function attains a maximal value of $S = 1$ for $|\alpha| = |\beta|$, decreases for $|\alpha| \neq |\beta|$ and approaches zero as one of the coefficients goes to zero. Intuitively, at least in the case of a pure state bi-partite system, the Von Neumann entropy serves as a proper measure of entanglement. The Bell states are then *maximally entangled*, as any other state possesses a smaller degree of entanglement. Separable states are the least entangled, with $S = 0$. It turns out, however, that for more complex systems the Von Neumann entropy does not properly measure the entanglement, especially for composite systems that are not pure states.

2.2 Entanglement Measures

The subset of Quantum Information Theory that is devoted to finding ways to measure the entanglement present in a quantum system is an extensive and evolving field. [33, 34, 35, 36, 32]. The problem is especially complicated in many-body systems

where the entanglement is not necessarily bi-partite, but instead may involve multiple sub-spaces. The classification and evaluation of proposed entanglement measures presents considerable technical challenges for even a small number of sub-systems[32]. On the other hand bi-partite entanglement is generally well defined and its measures are typically simple to compute. Furthermore, bi-partite entanglement is the critical resource in many applications of quantum information theory, where the successful application of a protocol usually depends upon the degree that two systems share an entangled pair. It is also the natural quantity to consider when examining the propagation of EPR pairs, and other types of excitations that will be encountered when the dynamical entanglement properties of quantum spin chains are examined later in this work.

To account for the calculation of bi-partite entanglement in a multi-partite system, consider the previous system composed of sub-systems A, B, and now additionally C. The task is to calculate the entanglement between systems A and B. This is accomplished by first tracing out C to find the reduced density matrix ρ_{AB}. In the case where $C = \mathbf{1}$, ρ_{AB} is a pure state, and the results of the previous section apply. However for $C \neq 1$ ρ_{AB} is a mixed state.

A bi-partite entanglement measure E may be defined as a mapping from the reduced density matrix ρ_{AB} to the real numbers. This measurement of entanglement $E(\rho_{AB})$ must necessarily satisfy the following conditions[37]

1. The entanglement $E(\rho_{AB}) = 0$ if and only if ρ_{AB} is a pure state

2. Given local unitary operations U_A and U_B, $E(U_B U_A \rho_{AB} U_A^\dagger U_B^\dagger) = E(\rho_{AB})$

3. The action of correlated local operations $V_{A,i}$ and $V_{B,i}$ on ρ_{AB} results in

$$E(\sum_i V_{B,i} V_{A,i} \rho_{AB} V_{A,i}^\dagger V_{B,i}^\dagger) \leq E(\rho_{AB}) \tag{2.11}$$

   In other words, local operations and classical commutation of operators (LOCC in quantum information theory) acting on subspace A or B cannot result in a increase in entanglement.

If ρ_{AB} a pure state, that is $C = 1$ above, then the unique entanglement measure that satisfies these conditions is the Von Neumann entropy introduced previously.

$$S(\rho_A) = -\mathrm{Tr}_B(\rho_{AB} \log_2 \rho_{AB}). \tag{2.12}$$

This measure is useful in a many-body system when the quantity of interest is the degree that one part of the system is entangled with the entirety of the rest. For example, the amount of entanglement a single spin shares all of the other spins in the chain, commonly called the *one-tangle* τ_1 [32].

When $C \neq 1$ the Von Neumann entropy is no longer a unique measurement of the entanglement. The reason for this is that whereas the Schmidt decomposition of a pure state is unique, there are infinitely many decompositions of the density matrix ρ_{AB} each of which give a different entropy. The usual method for arriving at a entanglement measure is to choose the decomposition that minimizes the entropy, resulting in the *entanglement of formation* E_F given by [38, 32]

$$E_F(\rho) = -\sum_{\sigma=\pm} \frac{\sqrt{1+\sigma C^2(\rho)}}{2} \ln \frac{\sqrt{1+\sigma C^2(\rho)}}{2} \tag{2.13}$$

where $C(\rho)$ is the *concurrence*

$$C(\rho_{A,B}) = \mathrm{Max}(0, \lambda_1 - \lambda_2 - \lambda_3 - \lambda_4). \tag{2.14}$$

In this formula, $\{\lambda_i\}$ are the eigenvalues of $\rho_{A,B}\sigma_y \otimes \sigma_y (\rho_{A,B})^* \sigma_y \otimes \sigma_y$ with $\lambda_1^2 \geq \ldots \geq \lambda_4^2$. The quantity C^2 is known as the *2-tangle* τ_2, and since E_F is a monotonic function of C, both the concurrence and the 2-tangle can also serve as entanglement measures. The concurrence has the additional intuitive property regarding the distribution of entanglement in $C^2_{A,B} + C^2_{A,C} \leq C^2_{A,(BC)}$[35].

It is worth mentioning that the amount of pure state entanglement required to create the state may be different from the amount of pure state entanglement one can extract from the state[39, 40, 41]. The extracted entanglement is an asymptotic limit related to the probability of obtaining a maximally entangled state from the mixed state, whereas the entanglement of formation E_F takes a fixed value related to the

number of maximally entangled states required to make form the mixed state. Using E_F has the advantage of being well-defined and easily calculable, and for this reason results related to bi-partite entanglement will be typically expressed in one of the monotones of E_F.

A final quantity that is useful in the analysis of entangled systems is the fidelity, which is the projection of the reduced density matrix onto a specific state $F^{\psi}_{A,B} = \mathrm{Tr}(\rho_{A,B} |\psi\rangle \langle\psi|)$. It be measured with respect to any state $|\psi\rangle$, but typically its use is as an indication of the evolution of the reduced density matrix from some initial state $|\psi(0)\rangle$, or as the projection onto some maximally entangled Bell states.

2.3 Dynamics Of Entanglement

One of the central themes of this work is the study of the dynamical properties of entanglement. In order to calculate how the various entanglement measures of a system evolve in time the reduced density matrix first needs to be calculated as it evolves from some initial state. Represent this state by $|\psi(0)\rangle$. Then there exists some unitary operator $U(H,t)$, dependent upon a specific model Hamiltonian so that the time evolution of the state of the system is given by

$$|\psi(t)\rangle = U(H,t) |\psi(0)\rangle . \tag{2.15}$$

Suppose the task is to compute the entanglement present in a subsystem A of the composite system $A \otimes N$. If $\{|\alpha_i\rangle\}$ and $\{|\eta_i\rangle\}$ are bases that span these systems, then the reduced density matrix $\rho_A(t)$ is

$$\rho_A(t) = \sum_i \langle\eta_i| U(H,t) |\psi(0)\rangle \langle\psi(0)| U^{\dagger}(H,t) |\eta_i\rangle . \tag{2.16}$$

Inserting resolutions of the identity operator yields

$$\rho_A(t) = \sum_{i,j,k} |\alpha_j\rangle \langle\alpha_j\eta_i| U(H,t) |\psi(0)\rangle \langle\psi(0)| U^{\dagger}(H,t) |\eta_i\alpha_k\rangle \langle\alpha_k| . \tag{2.17}$$

Since the $\{|\eta_i\rangle\}$ are a complete orthonormal set,

$$\rho_A(t) = \sum_{i,j} |\alpha_i\rangle \langle\psi(0)| U^{\dagger}(H,t) |\alpha_j\rangle \langle\alpha_i| U(H,t) |\psi(0)\rangle \langle\alpha_j| . \tag{2.18}$$

At this point it is necessary to specify some of the details of the system. Suppose that the subsystem A is a pair of spin 1/2 particles at positions m and n in a one-dimensional chain of N particles. A proper basis for A is then $\{|\alpha_i\rangle\} = \{|11\rangle, |10\rangle, |01\rangle, |00\rangle\}$. Also, assume that there exist fermionic operators c_m and $c_m^\dagger$ that act locally in the spin site m with the rules: $c_m |0_m\rangle = 0$, $c_m |1_m\rangle = |0_m\rangle$, $c_m^\dagger |0_m\rangle = |1_m\rangle$, $c_m^\dagger |1_m\rangle = 0$. The basis vectors may be written as a function of these fermionic operators

$$\begin{aligned}
|1_m 1_n\rangle &= \frac{1}{4}(c_m^\dagger c_m c_n^\dagger c_n + c_m^\dagger c_m c_n^\dagger + c_m^\dagger c_n^\dagger c_n + c_m^\dagger c_n^\dagger) \sum_i |\alpha_i\rangle \\
|1_m 0_n\rangle &= \frac{1}{4}(c_m^\dagger c_m c_n + c_m^\dagger c_m c_n c_n^\dagger + c_m^\dagger c_n + c_m^\dagger c_n c_n^\dagger) \sum_i |\alpha_i\rangle \\
|0_m 1_n\rangle &= \frac{1}{4}(c_m c_n^\dagger c_n + c_m c_n^\dagger + c_m c_m^\dagger c_n c_n^\dagger + c_m c_m^\dagger c_n^\dagger) \sum_i |\alpha_i\rangle \\
|0_m 0_n\rangle &= \frac{1}{4}(c_m c_n + c_m c_n c_n^\dagger + c_m c_m^\dagger c_n + c_m c_m^\dagger c_n c_n^\dagger) \sum_i |\alpha_i\rangle
\end{aligned} \tag{2.19}$$

which allow the density matrix $\rho_{m,n}(t)$ to be written

$$\rho_{(m,n)}(t) = \sum_{i,j} |\alpha_i\rangle \langle\psi(0)| C_{(m,n),j}(t) C^\dagger_{(m,n),i}(t) |\psi(0)\rangle \langle\alpha_j| , \tag{2.20}$$

where $C_{(m,n),i}$ and its conjugate is the i^{th} combination of the c_m and c_n operators in the expansion of the basis states above. If it is possible to express the Hamiltonian in terms of these raising and lowering operators and then find their time dependence, then the entanglement dynamics can, at least in principle, be computed by the evaluation of the correlation function dependent on the spin sites m and n averaged over the initial state of the system. The one dimensional spin 1/2 XY Heisenberg model is particularly suited to this sort of analysis and is the focus of the next chapter. It is a subset of the general Heisenberg model, which is

$$H = -\sum_{i,j} J_x S_i^x S_j^x + J_y S_i^y S_j^y + J_z S_i^z S_j^z - B \sum_i S_i^z. \tag{2.21}$$

The geometry of the chain can be taken to be either a line or ring, so that in the latter case $S^{\alpha}_{N+1} = S^{\alpha}_{1}$, where N is the number of sites in the chain. The nearest-neighbor XY model is the result of setting $j = i + 1$ and $J_z = 0$. If $J_y = 0$ in addition the resulting Hamiltonian is known as the Ising model. Other notable variants of this Hamiltonian have been studied as well, the isotropic Heisenberg model, the XXZ model, as well as models where either the couplings J_x, J_y, and J_z vary in time or space[32]. Furthermore, the geometry of the chain need not be a single line, multiple chains [42] or those inter-coupled in a ladder-like[43, 44] or other fashion[45] have been studied recently. The magnetic field B may be varied as well again either in time[46] or space[47, 48] and this latter situation will be addressed in the next chapter.

Other spin chain models not based upon the Heisenberg model include infinite range interaction models used to discuss entanglement between the spins in nuclei[49, 50, 51], frustrated spin 1/2 systems[52], and spin 1 chains[53]. While spin chains have received the bulk of the theoretical treatment of entanglement in the context of condensed matter systems, other notable models include strongly correlated fermionic systems[54], spin-boson models[55], and harmonic lattices[56].

Chapter 3

The XY Model

As briefly mentioned in the previous chapter, the one-dimensional XY model is a subclass of the general Heisenberg spin chain model. It has received considerable theoretical attention as it is one of the simplest non-trivial integrable models that can be used to study the universal behavior of low dimensional systems. It possesses a rich two dimensional phase diagram characterized by two separate quantum phase transformations, one belonging to the Ising universality class and the other of the Heisenberg universality class.

The statistical mechanics of the model are well known. A solution for the XY model in the absence of a magnetic field was first presented by Lieb, Schultz and Mattis [57] and in the presence of a magnetic field by Niemeijer [58, 59]. An extensive study of the model was put forth by Barouch, McCoy, et al. [60, 61, 62, 63] in which demonstrated the calculation of the fundamental correlation functions. Much later the model was revisited with the purpose examining entanglement present in the vicinity of the phase transitions [64, 65, 66]. More recently the dynamics of the model, and specifically of the entanglement, have become a subject of interest with ramifications in the field of quantum information science [22, 67, 48].

In this chapter, a review of the solution and phase diagram of the XY model in a constant field will be presented. These results will then be applied to a previously unconsidered case, the XY model with a staggered field. The dynamics of the entanglement in this system will be discussed and compared with previously known cases.

3.1 Diagonalization Of The Spin 1/2 XY Model In A Transverse Field

The spin 1/2 XY model in a transverse field is

$$H = -\lambda \left[\sum_{i=1}^{N} (1+\gamma) S_i^x S_{i+1}^x + (1-\gamma) S_i^y S_{i+1}^y \right] - \sum_{i=1}^{N} S_i^z. \tag{3.1}$$

The anisotropy parameter, $\gamma \in [0,1]$ may be adjusted to set the model as isotropic XX model ($\gamma = 0$), Ising ($\gamma = 1$) or anisotropic XY for a general value of γ. Furthermore, $\lambda = J/B$ is the ratio of the nearest neighbor exchange coupling to the local magnetic field. Of special importance is the sign of λ. For $\lambda > 0$ the spins tend to align and the chain is of the ferromagnetic (FM) type. On the contrary, for $\lambda < 0$ the spins tend to be anti-aligned and the spin interaction is antiferromagnetic (AFM). Unless otherwise specified, the geometry of the chain is that of a ring of an even number of spins, implying the periodic boundary condition $\sigma_{N+1}^{\alpha} = \sigma_1^{\alpha}$.

The standard technique to deal with such Hamiltonians of this type is to map the Spin 1/2 operators onto spinless fermionic operators. In the many-site problem this is accomplished via the Jordan-Wigner transformation[68]

$$\begin{aligned} \sigma_i^z &= 2c_i^\dagger c_i - 1 \\ \sigma_i^+ &= \prod_{j<i} (\sigma_j^z) c_i \\ \sigma_i^- &= \prod_{j<i} (\sigma_j^z) c_i^\dagger. \end{aligned} \tag{3.2}$$

In the basis where $|\uparrow\rangle_i$ and $|\downarrow\rangle_i$ represents a spin of $1/2$ and $-1/2$ in the $\hat{z}$ direction respectively, these states under the Jordan-Wigner transformation become $|0\rangle$ and $|1\rangle$.

Upon applying the Jordan-Wigner transformation the Hamiltonian is

$$H = -\frac{\lambda}{2} \sum_{i=1}^{N} (c_i^\dagger c_{i+1} + c_{i+1}^\dagger c_i + \gamma (c_i^\dagger c_{i+1}^\dagger + c_{i+1} c_i)) + \sum_{i=1}^{N} c_i^\dagger c_i - \frac{N}{2}. \tag{3.3}$$

The $\frac{N}{2}$ is a constant term and can be discarded. The next step in the diagonalization of the Hamiltonian is to take the Fourier transform to k space of H. It is

here where the parity of N plays a part. If N is odd, then the Fourier transform is performed in the context of the anti-periodic boundary condition σ^{α}_{N+1} = -σ^{α}_{1} as opposed to the periodic condition in the even N case. This results in ground state energy gap between the even and odd systems of $E_e - E_o \approx O(\frac{1}{N})$, which vanishes in the thermodynamic limit $N \to \infty$. The results of this work are calculated in the thermodynamic limit where $N > 100$, thus the assumption of even N, which facilitates the calculation of the Fourier transforms, is justified.

With this in mind, the Fourier transform $c_k = \frac{1}{\sqrt{N}} \sum_k c_i e^{-ikr_i}$ applied to the H yields

$$H = \sum_k \begin{pmatrix} c_k^\dagger & c_{-k} \end{pmatrix} \begin{pmatrix} A & iB \\ -iB & -A \end{pmatrix} \begin{pmatrix} c_k \\ c_{-k}^\dagger \end{pmatrix}, \tag{3.4}$$

where $A(k) = 1 - \lambda\cos(k)$ and $B(k) = \gamma\lambda\sin(k)$. Since the fermionic c operators are particle non-conserving, it is necessary to use a Bogoliubov transformation to diagonalize the Hamiltonian. To that end, a new fermionic operator b_k is introduced

$$b_k = u_k c_k + i v_{-k} c_{-k}^\dagger. \tag{3.5}$$

This is a canonical transformation provided that commutation relations are preserved. Without any restrictions on the coefficients both $\{b_k, b_l\} = 0$ and $\left\{b_k^\dagger, b_l^\dagger\right\} = 0$ are satisfied, however $\left\{b_k, b_l^\dagger\right\} = \delta_{k,l}$ requires that $u_{-k}u_k - v_{-k}v_k = 1$, which is satisfied by imposing that $u_k = u_{-k}$, $v_k = -v_{-k}$ and $u^2 + v^2 = 1$.

Under this transformation the Hamiltonian now reads

$$H = \sum_k \begin{pmatrix} b_k^\dagger & b_{-k} \end{pmatrix} \begin{pmatrix} u_k & iv_{-k} \\ -iv_k & u_{-k} \end{pmatrix} \begin{pmatrix} A & iB \\ -iB & -A \end{pmatrix} \begin{pmatrix} u_k & iv_{-k} \\ -iv_k & u_{-k} \end{pmatrix}^{-1} \begin{pmatrix} b_k \\ b_{-k}^\dagger \end{pmatrix}. \tag{3.6}$$

The requirement that H be diagonal in the Bogoliubov basis fixes u_k and v_k so that the Hamiltonian takes the form

$$H = \sum_k \omega_k (b_k^\dagger b_k - 1/2), \tag{3.7}$$

with $\omega_k = \sqrt{A_k^2 + B_k^2}$. The transform coefficients u_k and v_k are determined to be

$$\begin{aligned} u_k &= \frac{\omega_k - A_k}{\sqrt{2\omega_k(\omega_k - A_k)}} \\ v_k &= \frac{B_k}{\sqrt{2\omega_k(\omega_k - A_k)}}. \end{aligned} \tag{3.8}$$

With the energy spectrum in hand the thermodynamics of the model as well as the corresponding $D+1$ classical model may be computed[4].

3.1.1 Time Dependence

The time dependence of the b_k operator is given by $\partial b_k/\partial t = i[H, b_k]$ which gives $b_k(t) = e^{-i\omega_k t} b_k(0)$. The time dependence of the Jordan-Wigner operator $c_k(t)$ is given by the inverse of 3.5, namely $c_k(t) = u_k b_k(t) - i v_k b^\dagger_{-k}(t)$. This gives the intermediate result

$$c_k(t) = e^{-i\omega_k t}\left[u_k^2 c_k(0) + v_k^2 c_k^\dagger(0) + i(u_k v_{-k} c^\dagger_{-k}(0) - u_{-k} v_k c_{-k}(0))\right]. \tag{3.9}$$

In order to calculate the correlation functions which are the matrix elements of the reduced density matrix 2.20, the position-space representation of this operator is required. After a Fourier transform $c_m(t) = \frac{1}{N}\sum_{n=1}^{N} \alpha_{n-m}(t) c_n(0) - i\beta_{n-m}(t) c_n^\dagger(0)$ with time dependent coefficients

$$\begin{aligned} \alpha_n(t) &= \sum_k \cos(kn)(e^{i\omega_k t} u_k^2 + e^{-i\omega_k t} v_k^2) \\ \beta_n(t) &= 2\sum_k \sin(kn) u_k v_k \sin(\omega_k t), \end{aligned} \tag{3.10}$$

where the previously suppressed overall factor $\frac{1}{N}$, due to the discrete Fourier transforms, has been included to reflect the way these operators are to be handled in a computer program. This is the main result that allows the calculation of the density matrix elements introduced in 2.20 for the XY model in a uniform field.

A simplification may be made in the case of the $\gamma = 0$ isotropic XX model in the $N \to \infty$ thermodynamic limit. Using the result[69]

$$J_n(z) = \frac{i^{-n}}{\pi}\int_0^\pi \cos(n\theta) e^{iz\cos\theta} d\theta, \tag{3.11}$$

it is possible to write

$$c_m(t) = e^{it}\sum_{n=1}^{N} i^{n-m} J_{n-m}(\lambda t) c_{n-m}(0), \tag{3.12}$$

which suggests that excitations propagate through the chain at speed $\pm\lambda$ for this special case.

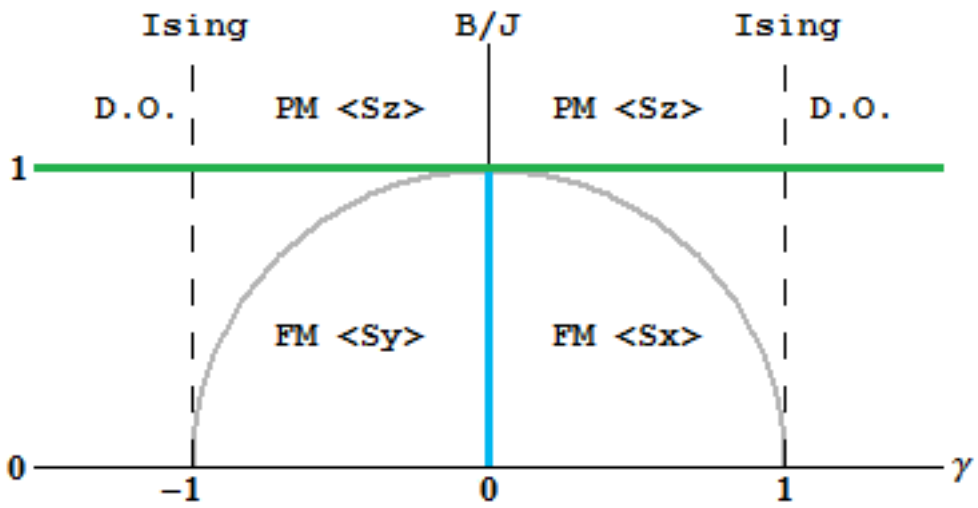

Figure 3.1: Phase diagram for a the spin 1/2 XY chain in a uniform transverse magnetic field.

3.1.2 Phase Diagram

The zero-temperature phase diagram of the spin 1/2 XY chain in a uniform transverse field is shown in figure 3.1. Two distinct quantum phase transitions are represented. The line $1/\lambda = 1$ separates the ferromagnetic ordered ground-state phase (FM) for $1/\lambda < 1$ from the paramagnetic quantum disordered phase (PM). The other transition occurs along the line $\gamma = 0$ for $0 < 1/\lambda < 1$ an is the boundary between ferromagnetic ordering in the $\hat{x}$ direction for $\gamma > 0$ and ferromagnetic ordering in the $\hat{y}$ direction for $\gamma < 0$. Each of these lines possess a vanishing energy gap Δ. The quantum phase transition along $1/\lambda = 1$ is the Ising transition whereas the other transition along $\gamma = 0$ is the anisotropy transition. Both of these quantum phase transitions are of second order but not of the same universality class, for example the critical exponent η which describes the behavior of the ground state correlation function $\langle \sigma_r^x \sigma_0^x \rangle \sim r^{1-\eta}$ is $\eta = 5/4$ for the Ising transition at $\gamma = 1$ but $\eta = 3/2$ for the anisotropy transition at $B = 0$[70].

The contour $\gamma^2 + 1/\lambda^2 = 1$ corresponds to the case where the wave function of the ground state is factorized into a product state of single spin states[71, 72]. Specifically,

along this contour the ground state is generally doubly degenerate, and has the form

$$\begin{aligned} |\psi_1\rangle &= \cos\theta \sum_{j=1}^{N} (|\downarrow_j\rangle + \tan\theta\, |\uparrow_j\rangle) \\ |\psi_2\rangle &= \cos\theta \sum_{j=1}^{N} (|\downarrow_j\rangle - \tan\theta\, |\uparrow_j\rangle), \end{aligned} \tag{3.13}$$

where $\cos^2(2\theta) = (1-\gamma)/(1+\gamma)$.

The notable case where $\gamma = 0$ and $1/\lambda = 1$ takes has the form $|\psi\rangle = \sum_{j=1}^{N} |\downarrow\rangle \equiv |\Downarrow\rangle$. As the field is increased further the ground state remains the same, since $\Delta > 0$ for $\lambda < 1$.

3.2 Spin 1/2 XY Model In A Staggered Transverse Field

The Hamiltonian of the XY model in a constant transverse field 3.1 may be modified to include other time independent spatial field configurations.

$$H = -\lambda \left[\sum_{i=1}^{N} (1+\gamma) S_i^x S_{i+1}^x + (1-\gamma) S_i^y S_{i+1}^y \right] - \sum_{i=1}^{N} \mathbf{b}_i \cdot \mathbf{S}_i \tag{3.14}$$

If $\mathbf{b}_i = (-1)^i \hat{z}$ then the field is again transverse, but has alternating direction with the field in the $-\hat{x}$ direction for odd sites and the $\hat{x}$ direction for even sites. Other configurations are of course possible, but generally result in non-integrable models. If $\mathbf{b}_i$ has an $\hat{x}$ or $\hat{y}$ component the resulting Hamiltonian after a Jordan-Wigner transform will contain quartic contributions in the Jordan-Wigner fermions. On the other hand, if $\mathbf{b}_i$ contains only components in the $\hat{z}$ direction but is anything but a staggered or uniform configuration, the Fourier transform of the Jordan-Wigner transformed Hamiltonian cannot be written in a closed form. A subsequent calculation on a computer would thus require, in general, N times as many operations to compute a correlation function. In this work, discussion of spatially non-uniform fields will then be limited to the staggered field. Both for reasons of technical necessity, but also because a staggered magnetic field may arise naturally by a chain of spins in proximity to an anti-ferromagnet.

The XY model in a staggered field may be brought into a similar form of the uniform field case (Eq. 3.1) under a π-rotation about the $\hat{x}$ axis on every other site. Specifically by means of the rotation

$$X = \prod_i \hat{R^x_{2i+1}}(\pi), \tag{3.15}$$

the spin operators are transformed

$$\begin{aligned} \hat{S}^x_i &\rightarrow \hat{S}^x_i \\ \hat{S}^{y,z}_{2i} &\rightarrow \hat{S}^{y,z}_{2i} \\ \hat{S}^{y,z}_{2i+1} &\rightarrow -\hat{S}^{y,z}_{2i+1}. \end{aligned} \tag{3.16}$$

The Hamiltonian of the XY-model in a staggered transverse field transforms into one resembling the uniform field XY model, amenable to the analysis of the previous section. The resulting Hamiltonian $H^{(R)}$ is

$$H^{(R)} = \gamma\lambda \sum_{i=1}^{N} (1+\frac{1}{\gamma}) S^x_i S^x_{i+1} + (1-\frac{1}{\gamma}) S^y_i S^y_{i+1} - \sum_{i=1}^{N} S^z_i. \tag{3.17}$$

An alternative way of looking at this transformation is that a XY chain with antiferromagnetic $\hat{x}$ and $\hat{y}$ couplings at arbitrary $\gamma \neq 0$ with a staggered field may be transformed into the FM uniform field model by a simple rescaling: $\hat{X}\hat{H}(\lambda, \gamma, (-1)^i)\hat{X^{-1}} = \hat{H}(-\gamma\lambda, 1/\gamma, 1)$. The same diagonalization procedure as used in the constant field case may now be applied, resulting in a dispersion for the rotated Bogoliubov operators $b^{(R)}_i$, $\omega^{(R)}_k = \sqrt{A^{2(R)} + B^{2(R)}}$, except now

$$\begin{aligned} A^{(R)}_k &= 1 - \gamma\lambda\cos(k) \\ B^{(R)}_k &= \lambda\sin(k). \end{aligned} \tag{3.18}$$

The Bogoliubov coefficients have the same form, as does the time dependence of the model, just with appropriate substitutions for the rotated $A^{(R)}_k$ and $B^{(R)}_k$ so that,

$$\begin{aligned} u^{(R)}_k &= \frac{\omega^{(R)}_k - A^{(R)}_k}{\sqrt{2\omega^{(R)}_k(\omega^{(R)}_k - A^{(R)}_k)}} \\ v^{(R)}_k &= \frac{B^{(R)}_k}{\sqrt{2\omega^{(R)}_k(\omega^{(R)}_k - A^{(R)}_k)}}. \end{aligned} \tag{3.19}$$

The time dependence of the $c_m^{(R)}$ operator is, $c_m^{(R)}(t) = \frac{1}{N}\sum_{n=1}^{N} \alpha_{n-m}^{(R)}(t) c_n^{(R)}(0) - i\beta_{n-m}^{(R)}(t) c_n^{\dagger(R)}(0)$ with time dependent coefficients

$$\begin{aligned} \alpha_n^{(R)}(t) &= \sum_k \cos(kn)(e^{i\omega_k^{(R)}t} u_k^{2(R)} + e^{-i\omega_k^{(R)}t} v_k^{2(R)}) \\ \beta_n^{(R)}(t) &= 2\sum_k \sin(kn) u_k^{(R)} v_k^{(R)} \sin(\omega_k^{(R)} t), \end{aligned} \tag{3.20}$$

The apparent similarity between the equations for the staggered field and uniform field cases is deceptive, as can be immediately noticed by considering the thermodynamic limit when $\gamma =$ and $\lambda \ll 1$. In this regime the sum over k in the equation for α may be evaluated exactly and the evolution coefficients become

$$\begin{aligned} \alpha_n(t) &\approx \begin{cases} i^{-n/2} J_{n/2}(\frac{\lambda^2}{4} t) & \text{, n even} \\ 0 & \text{, n odd} \end{cases} \\ \beta_n(t) &\approx \frac{\lambda}{N} \sum_k \sin(kn) \sin(k) \sin(\omega_k t) \end{aligned} \tag{3.21}$$

where $J_n(x)$ is the Bessel function of the first kind. This allows us to write the Jordan-Wigner operator for the isotropic, strong staggered field configuration as

$$c_m(t) \approx \sum_n i^{-(n-m)} J_{(n-m)/2}(\lambda^2 t/4) c_n, n\text{-}m \text{ even}. \tag{3.22}$$

The coefficients in of the c_k in Eq. 3.12 and 3.22 indicate that, in the appropriate limiting cases, excitations above the ground state, or the Néel state in the case of Eq. 3.22, propagate through the chain with a Bessel-like profile at apparent speed λ and λ^2 respectively. Since λ has no first order contribution in dependence in Eq. 3.22 for the staggered field configuration, the sign of the interaction does not play a significant role. The sum in Eq. 3.22 receives its dominant contribution from the sites on the same sublattice thereby indicating that the spin wave is confined to one sublattice. In contrast, the uniform field case Eq. 3.12 does not distinguish between even and odd sites. Finally, the shape of the wave shows some broadening, which stems from a redistribution of the spectral weight among the different states that the wave packet is composed of, thereby manifesting a decoherence characteristic of any state different from a purely stationary one.

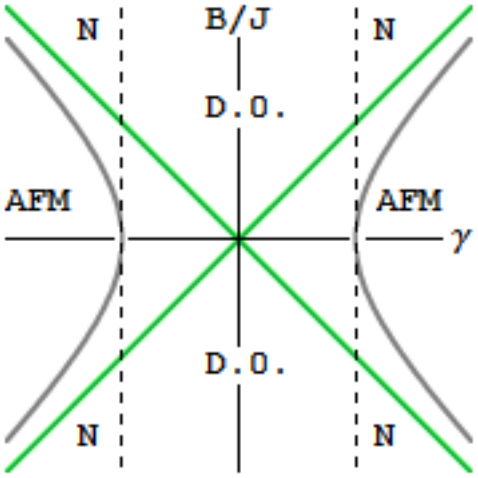

Figure 3.2: Phase diagram for the spin 1/2 XY chain in a staggered transverse magnetic field. AFM indicates the ground state of a quantum anti-ferromagnet, N indicates the Néel phase, and D.O. is a disordered phase.

3.2.1 Phase Diagram

Given the mapping between the uniform field and staggered field spin 1/2 XY models established in the previous section, namely the rotation which takes $-\gamma\lambda \to \lambda'$ and $\gamma \to 1/\gamma'$, the phase diagram for the staggered field model can be constructed. The ground states also must be rotated so that a region with $\langle S^z \rangle = 1$ becomes the Néel state defined as $|\psi_N\rangle = |\downarrow\uparrow\downarrow \ldots\rangle \equiv |\Updownarrow\rangle$. The areas that previously were ferromagnetic ground states $\langle S^x \rangle \neq 0$ and $\langle S^y \rangle \neq 0$ are now some antiferromagnetic ground state. The diagram is shown in figure 3.2.

In the region $\gamma \in (-1, 1)$ the state of the system is either in an AFM ground state for $|\gamma| > |h|$, or a disordered state otherwise. For increasing values of h the ground state approaches the Néel state. Along the lines $\gamma = 1$ and $\gamma = -1$ the Ising model is restored. Outside of this region a QPT exists at $|h| > |\gamma|$ that is isomorphic to the transition between the ferromagnetic and paramagnetic transition for the uniform field case. There is no transition in the staggered field case that corresponds to the anisotropy QPT of the uniform field model as γ' goes from 0_+ to 0_- as these points are at $+\infty$ and $-\infty$ respectively in the staggered field phase diagram.

These models are generally limited to $\gamma \in [-1, 1]$ in order to preserve the sign of the $\hat{x}$ and $\hat{y}$ interactions and in this region it is clear that the uniform field model has a much more robust phase diagram. Indeed the staggered field model, with its

antiferromagnetic interaction terms does not exhibit a transition between two ground states where an obvious order parameter, such as $\langle S^z \rangle$ undergoes a dramatic change. However, qualitatively, a distinction can be made between the ground state for $|h| > |\gamma|$, with its Néel-like ordering, as opposed to the $|h| < |\gamma|$ region which resembles the ground state of the zero-field quantum anti-ferromagnet.

3.3 Density Matrix And Correlation Functions

With the time dependence of the Jordan-Wigner fermion operators $c_i(t)$ known it is possible to compute the evolution of the reduced density matrix $\rho_{m,n}(t)$, described previously (Eq. 2.20). The composite operators $C_{m,n}$ and $C^\dagger_{m,n}$ may now be evaluated given the basis $\{|\uparrow\uparrow\rangle, |\uparrow\downarrow\rangle, |\downarrow\uparrow\rangle, |\downarrow\downarrow\rangle\}$, which results in the density matrix

$$\rho^{(2)}_{m,n}(t) = \begin{pmatrix} \langle P^+_m P^+_n \rangle & \langle P^+_m \sigma^-_n \rangle & \langle \sigma^-_m P^+_n \rangle & \langle \sigma^-_m \sigma^-_n \rangle \\ \langle P^+_m \sigma^+_n \rangle & \langle P^+_m P^-_n \rangle & \langle \sigma^-_m \sigma^+_n \rangle & \langle \sigma^-_m P^-_n \rangle \\ \langle \sigma^+_m P^+_n \rangle & \langle \sigma^+_m \sigma^-_n \rangle & \langle P^-_m P^+_n \rangle & \langle P^-_m \sigma^-_n \rangle \\ \langle \sigma^+_m \sigma^+_n \rangle & \langle \sigma^+_m P^-_n \rangle & \langle P^-_m \sigma^+_n \rangle & \langle P^-_m P^-_n \rangle \end{pmatrix}. \tag{3.23}$$

In this equation, $P^\pm_m = \frac{1}{2}(1 \pm \sigma^z_m)$ are the projection operators, and σ^z_m, $\sigma^+_m = \frac{1}{\sqrt{2}}(\sigma^x + i\sigma^y)$, and $\sigma^-_m = \frac{1}{\sqrt{2}}(\sigma^x - i\sigma^y)$ are written in terms of the Jordan-Wigner fermionic $c(t)$ operators using Eq. 3.2.

To calculate the evolution of the density matrix it is necessary to specify the state over which the correlation functions that comprise the individual elements of the density matrix are averaged. The simplest non-trivial state to work with is the initial state where all of the spins in the chain are aligned with the transverse magnetic field, except for a few selected sites. For an initial state of a singlet shared between sites i and j and all the other sites aligned with a uniform field this is

$$|\psi_{i,j}\rangle = \frac{1}{\sqrt{2}}(c^\dagger_i(0) - c^\dagger_j(0))\,|\Downarrow\rangle\,. \tag{3.24}$$

The time dependent matrix elements are averaged over this state may be written as

$$\left\langle \psi_{i,j} \left| U^\dagger F(\sigma^\pm_m, \sigma^\pm_n) U(t) \right| \psi_{i,j} \right\rangle =$$

$$= \frac{1}{2}\left\langle \Downarrow \left| (c_i(0) - c_j(0)) F(\sigma(t)_m^{\pm}, \sigma(t)_n^{\pm})(c_i^\dagger(0) - c_j^\dagger(0) \right| \Downarrow \right\rangle, \tag{3.25}$$

where the functional form of F is determined by its position in the density matrix described above. Since the time dependence of the $c_i(t)$, and by extension the $\sigma_i^{\pm}(t)$ are known this is a calculable quantity.

These multi-point correlation functions may be decomposed Wick's Theorem, however for large $|m-n|$ this method becomes computationally intractable since they reduce to a sum of $\prod_i^{|m-n|}(2i-1)$ 2-point correlation functions. Alternatively, it is possible to write these correlation functions as a sum of Pfaffians [21], which may be computed as a sum of of $2|m-n| \times 2|m-n|$ dimensional Toplitz determinants.

The situation is similar for the staggered magnetic field, except one must account for the rotation as well. The initial state with a singlet on sites i and j has the form

$$|\xi_{i,j}\rangle = \frac{1}{\sqrt{2}}(c_i^\dagger + c_i - (c_j^\dagger + c_j))\,|\Updownarrow\rangle\,. \tag{3.26}$$

Also, since $|\xi_{i,j}\rangle = X^{-1}|\psi_{i,j}\rangle$ for the rotation X about $\hat{x}$ described in Eq. 3.15, the matrix elements of $\rho_{m,n}(t)$ becomes

$$\begin{aligned} &\left\langle \psi_{i,j} \left| XF(\sigma_m^{\pm}(t), \sigma_n^{\pm}(t))X \right| \psi_{i,j} \right\rangle \\ &= \frac{1}{2}\left\langle \Downarrow \left| (c_i(0) - c_j(0)) F(\sigma(t)_m^{\pm(R)}, \sigma(t)_n^{\pm(R)})(c_i^\dagger(0) - c_j^\dagger(0) \right| \Downarrow \right\rangle. \end{aligned} \tag{3.27}$$

With the time evolution of the reduced density matrix in hand, it is finally possible to compute the various measures of entanglement discussed in the preceding chapter. For general γ and λ a computer program is required to do this, since the correlation functions are too complicated to compute manually. The computer algorithm used to produce the results that appear in this work calculates the correlation functions by using the Wick technique to break up the generally multi-point functions in to two-point correlation functions, which are then evaluated individually and summed. This works well as long as the distance between observation sites is small, $|m-n| \lesssim 10$. However, if the time evolution of the $c_i(t)$ is a function of the $\sum_j c_j(0)$ only (and not $\sum_j c_j^\dagger(0)$), which corresponds to situations where the β terms are zero and the α terms are weighted sums of Bessel functions, (Eq. 3.12 and 3.22) then it is possible to

drastically reduce amount of computation required to calculate entanglement measures from the density matrix. Specifically if $|\Psi(t)_{i,j}\rangle = \sum_l w(t)_l c_l^\dagger(0)\,|\Downarrow\rangle$, where $|\Downarrow\rangle$ is the true ground state of the system, then the concurrence takes the form $C(t)_{m,n} = 2\,|w(t)_m w(t)_n|$ [22]. This number of operations required to compute this result is independent of $|m-n|$, so for $\gamma = 0$ the entanglement between well-separated spin sites may be computed for all λ for a uniform field, and approximately in the case $\lambda \ll 1$ for the staggered field configuration.

3.4 Entanglement Dynamics Of The XY Model

With the machinery of the previous sections in place it is now possible to calculate the evolution of the XY model density matrix, and therefore how various entanglement measures evolve in time. The dynamical properties of the entanglement in a uniform field XY system have already been extensively studied [21, 22, 32]. The staggered field configuration has received less attention [48] and this model will be the primary focus for the remainder of this chapter.

3.4.1 Evolution Of An EPR Pair

As previously mentioned, and EPR pair may be represented as a pair of entangled spin states, prepared in some initial state (usually one of the Bell states) that then propagate away from each other. As these spins propagate away from each other they may interact with their environment and thereby become less entangled. This process is generally called *decoherence* and is a major limiting factor in the successful implementation of quantum information protocols.

This situation may be simulated in the XY model by establishing a maximally entangled state on sites $i = -x_0$ and $j = +x_0$ and then examining the concurrence $C(t)_{-x,x}$. For $\gamma = 0$ this is computed exactly in the case of the uniform field model, but an approximate solution is only possible for the staggered field configuration for $\lambda \ll 1$, or the region of the phase diagram where the ground state is effectively the Néel state.

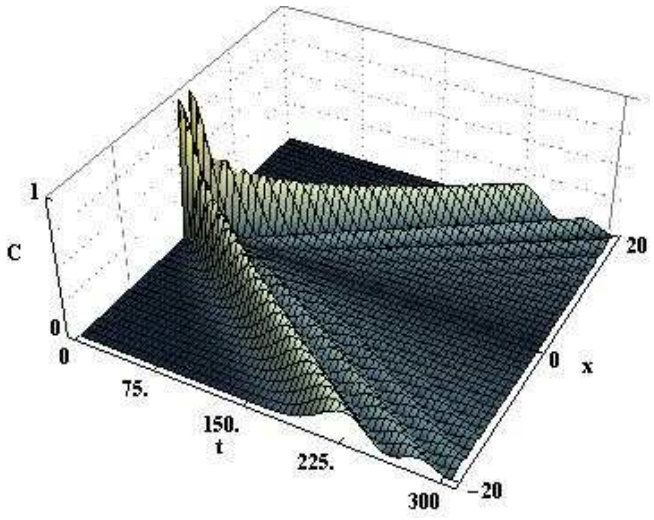

Figure 3.3: Evolution of EPR pair concurrence $C_{-x,x}$ for spin singlet state initially on sites (-1,1), uniform field, $\lambda = 0.1$, $\gamma = 0$

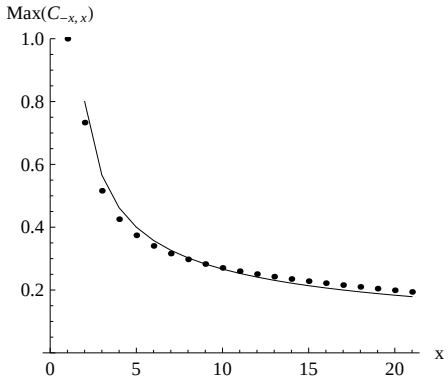

Figure 3.4: Maximal concurrence of EPR pair Max($C_{-x,x}$) for spin singlet state initially on sites (-1,1), staggered field, $\gamma = 0$. Fitted line proportional to $x^{1-\eta}$, with $\eta = 1.5$

The evolution of the EPR pair, in this case a singlet pair, is shown in Fig. 3.3 for the uniform field configuration. The spin singlet is initially shared between sites $(-1, 1)$, and has an concurrence $C(0)_{-1,1} = 1$ indicating the presence of a maximally entangled state. As the system evolves, the excitation propagates with speed $\sim \lambda$ in the $+x$ and $-x$ direction. The concurrence $C(t)_{-x,x}$ shows that the excitations traveling in each direction are entangled with each other, although not maximally, as they propagate. Furthermore, the entanglement between the pair decreases as the pair travels through the chain (losing entanglement as the spins interact with their 'environment', which is taken to be the other spins in the chain).

The amount of maximal entanglement lost as the spatial separation of the EPR pairs increases apparently follows a power law (Fig. 3.4). This plot is made by plotting

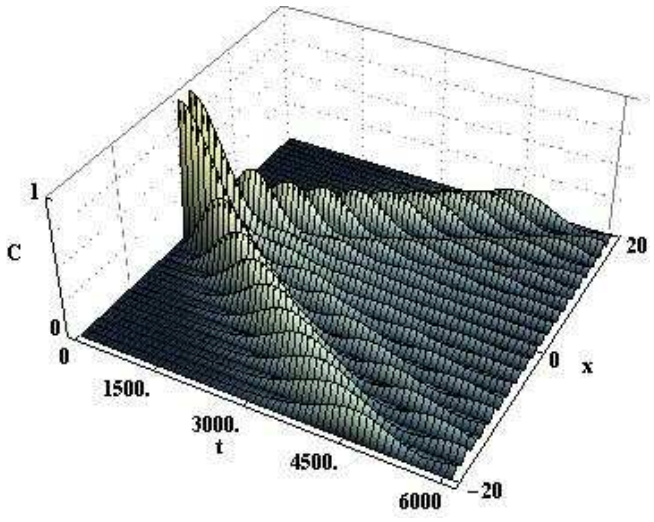

Figure 3.5: Evolution of EPR pair concurrence $C_{-x,x}$ for spin singlet state initially on sites (-1,1), staggered field, $\lambda = 0.1$, $\gamma = 0$

the maximum concurrence $C_{-x,x}$ as the EPR excitation passes through spin site x, and then plotting that versus the site. In effect, it is the spatial decoherence profile for the EPR pair and is proportional to the function $x^{1-\eta}$ with $\eta = 3/2$ for all values of λ when $\gamma = 0$. This is reminiscent of the power law dependence of the $\left\langle S_i^x S_j^x \right\rangle \sim |i-j|^{-1/2}$ correlation function for the XY anisotropy QPT, but in fact formally appears as the $x^{-1/2}$ decay of the maxima of the Bessel function. The exponent in the power law dependence of the maximal concurrence on site x serves as a convenient measure of the ability to transmit entangled states, with the asymptotic maxima of $\eta = 3/2$.

A similar situation, except with a staggered transverse field is shown in Fig. 3.5. Again the entangled EPR excitations are apparent but with several notable exceptions that are representative of the staggered field XY model in general, for $\gamma = 0$. As predicted in equation Eq. 3.22, the speed of the spin wave excitations is $\sim \lambda^2/4$. Also, the entanglement is confined to the sublattice shared by the two initial entangled spins, in this case the odd spins. This is again a consequence of Eq. 3.22 as $\alpha_j = 0$ if $\mathrm{mod}_2(i-j) \neq 0$.

Unfortunately in the staggered field case, this method is only approximately valid for $\lambda \ll 1$ so it is computationally difficult to make a comparative study of the chain to transfer EPR pairs as λ is varied, not to mention when γ is varied is well, in which case

this Bessel function approximation fails for both staggered and constant field models. Furthermore, even for $\lambda \sim 0.1$ and $\gamma = 0$, the Néel state is not the actual ground state of the system, as has been assumed in the computation of the concurrence. The presence of 'vacuum excitations' has therefore been ignored, which when accounted for properly, substantially alter the character of the transmitted entanglement. However the general properties, namely the speed and lattice characteristics of the entanglement propagation, evidence themselves for a wide range of λ and γ.

Without other approximations, the concurrence must be calculated on sites that are spatially close. This is exactly the situation that is appropriate to examine if it is desired to transfer a quantum state initially localized in one small part of the chain, for example neighboring spins, to two other neighboring spins at some other place in the chain.

3.4.2 State Transfer - Flying Qubits

With no limits on λ and $\gamma \in [0, 1]$, the matrix elements of $\rho(t)_{x,x+n}$ must be calculated using the full machinery described in this chapter, which is computationally tractable only for small n. It is an appropriate technique to examine the dynamical entanglement properties of state transfer, where the movement of a localized entangled state from one part of the chain to another is of primary interest. These localized entangled states that travel through the system are sometimes called *flying qubits*.

The concurrence $C_{i,i+n}$ is plotted in Fig. 3.6 for the $\lambda = 0.5$, $\gamma = 0$ uniform field configuration. The initial state has a single entangled pair on sites $(0, 1)$ in the spin singlet state. Again, the speed of the propagation of the wave is $\sim \lambda$, and the maximal concurrence between sites $(x, x + 1)$ as the flying qubit travels through the chain is found to be $\mathrm{Max}(C_{x,x+i}) = \frac{1}{2}x^{1-\eta}$ with $\eta = 3/2$.

If a similar plot $C_{x,x+2}$ is made for the staggered field configuration, with the modification that the initially entangled sites are (0,2) so that they are on same sublattice, it is clear that the quality of the state transfer is degraded (Fig. 3.7). As expected, the entanglement is again confined to the sublattice of the initial entangled

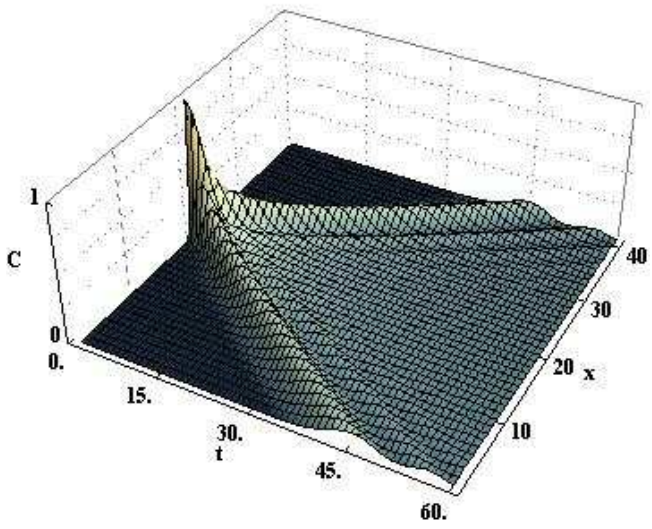

Figure 3.6: Evolution concurrence $C_{i,i+1}$ for entangled state initially on sites (0,1), uniform field, $\lambda = 0.5$, $\gamma = 0$

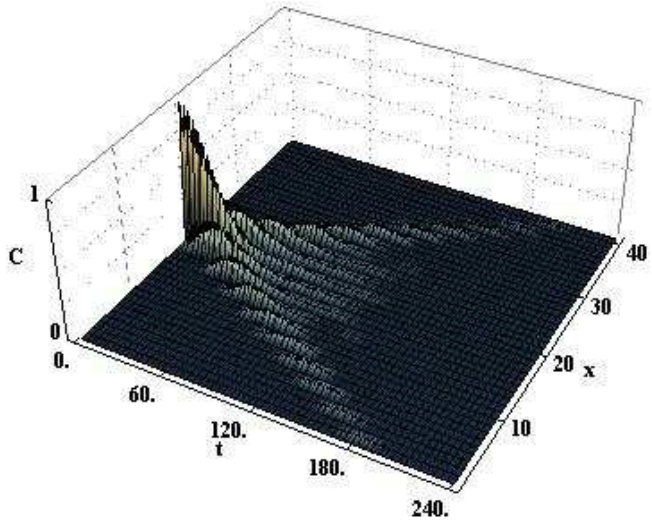

Figure 3.7: Evolution concurrence $C_{i,i+2}$ for entangled state initially on sites (0,2), staggered field, $\lambda = 0.5$, $\gamma = 0$

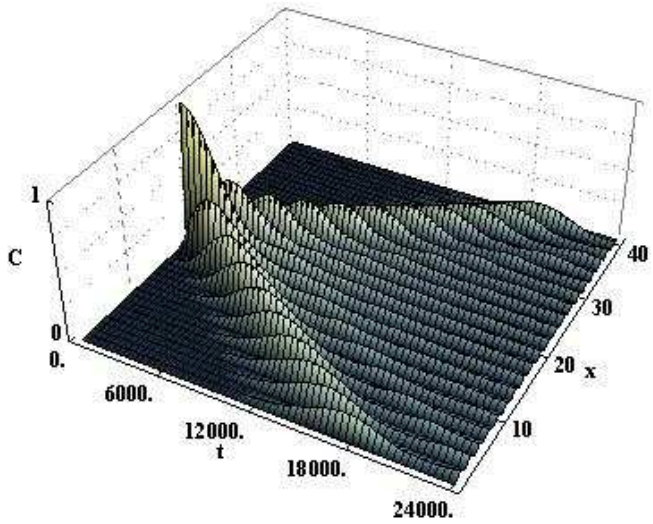

Figure 3.8: Evolution concurrence $C_{i,i+2}$ for entangled state initially on sites (0,2), staggered field, $\lambda = 0.05$, $\gamma = 0$

spins, and the speed of the transfer is $\sim \lambda^2$. If λ is decreased by an order of magnitude (Fig. 3.7) it is seen that the quality is restored at the expense of the speed at which the entanglement is transferred.

Evidently, as the ground state of the staggered field model approaches a true Néel state, that is as $h \to \infty$ or $\lambda \to 0$, the quality of the transmitted state increases. In fact, as shown in Fig. 3.9, which displays a comparison of the concurrence for the staggered field $\lambda = 0.5$ and $\lambda = 0.05$ models to the constant field configuration, as $\lambda \to 0$ the concurrence and fidelity of the transferred state approaches the maximal case of the constant field configuration.

Figures 3.9(a) and 3.9(b) demonstrate this behavior more clearly for $C_{i,i+2}$ and $F_{i,i+2}$ for the isotropic staggered and uniform field models with $\lambda = 0.05$ and 0.5, respectively. In the plots, the initially entangled pair is on the sites (0,2) while the fidelity and concurrence are computed on the sites (2,4) and (6,8). In the strong-field limit, the quality of entanglement transport in the staggered field model approaches that of the uniform field one (the dashed lines). The higher-frequency oscillations in the plots should be attributed to the fact that for any finite λ the unentangled initial

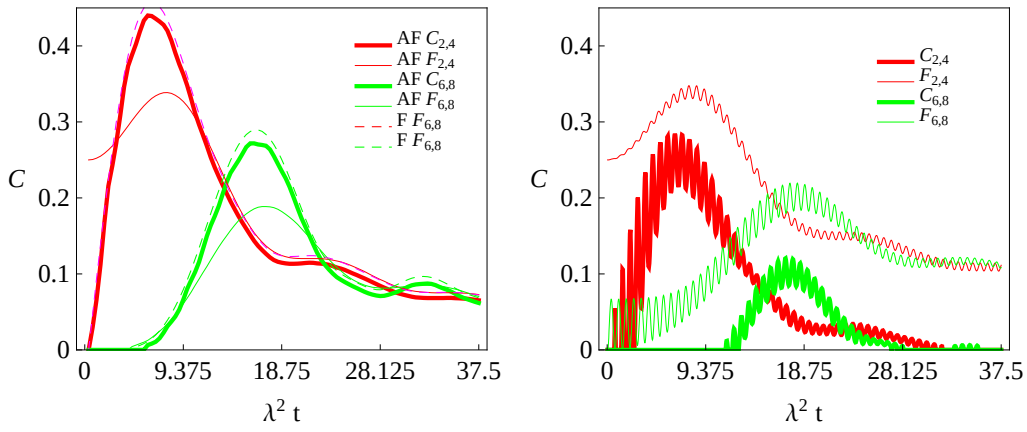

(a) $\lambda = 0.05$ (b) $\lambda = 0.5$

Figure 3.9: Concurrence $C_{i,i+2}$ and fidelity $F_{i,i+2}$, i sites removed from the initially entangled site at (0,2), for the staggered field model with $\gamma = 0$. The dashed lines represent the results obtained for a uniform field.

(classical Néel) state differs from the true ground one, and, therefore, in the course of its time evolution it exhibits vacuum fluctuations of entanglement even in the absence of any additional entangled pairs.

Related to the underlying staggered sublattice structure, the spatial period of these oscillations is twice the lattice spacing, while their amplitude is governed by the square of the function $\beta_j(t)$ (Eq. 3.21), and thus is proportional to λ^2. With increasing λ these vacuum fluctuations become more prominent and, concomitantly, the amount of transmitted entanglement decreases. While the singlet fidelity remains approximately constant, this reduction of the entanglement transfer is due to the emergence of additional states of the form a $a\,|{\uparrow\downarrow}\rangle + b\,|{\downarrow\uparrow}\rangle$, whose contribution is again governed by the coefficients $\beta_j(t)$ λ.

An analysis of the decoherence profile as a function of λ (Fig. 3.10) shows that for $\lambda \gtrsim 0.6$, these intrinsic decohering effects become so strong that an initially entangled state decays almost immediately. Additionally, at some $\lambda \sim 0.25$ the concurrence begins to diverge from a power-law behavior. The usefulness of the staggered field configuration as a entanglement transport medium in this regime is diminished. Instead, it is clear that only in the presence of a strong field can the isotropic staggered field model be a high-fidelity carrier of an entangled state, where it approaches the

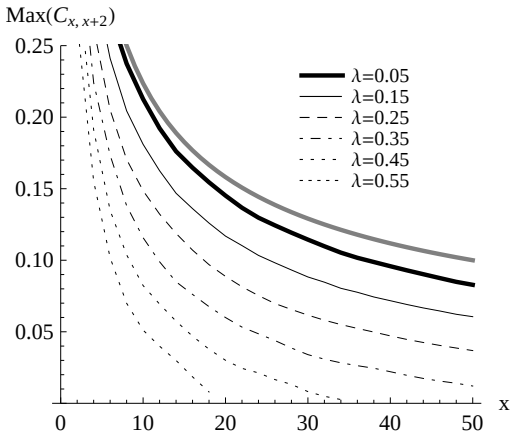

Figure 3.10: Maximal concurrence $C_{x,x+2}$ for varying λ. The thick gray line represents $x^{1-\eta}$ for $\eta = 3/2$.

capabilities of the constant field case.

3.4.3 Multiple Singlet Pairs

Next, an additional pair of entangled spins is placed some sites removed from the first pair. Formally, the initial is now represented by the equation

$$\xi_{i,j,k,l} = \frac{1}{2}(c_i^\dagger + c_i - (c_j^\dagger + c_j))(c_k^\dagger + c_k - (c_l^\dagger + c_l))\,|\Updownarrow\rangle\,. \tag{3.28}$$

The evolution of the system is shown in Fig. 3.11 for two cases where the entangled pairs are placed on the same and different sublattices. Specifically, in the left picture, $(i,j),(k,l) = (24,26),(47,49)$ and the same in the right picture $(i,j),(k,l) = (24,26),(46,48)$. The brighter areas indicate greater values of the nearest sublattice-neighbor concurrence.

The outward-moving entanglement waves propagate away from the initially entangled sites with the same speed λ^2 as in the one-singlet case. The lack of any detectable concurrence among nearest lattice-neighbor sites in the sublattice not containing the initially entangled sites is a direct consequence of Eq. 3.21, in the strong-field limit. The other two inward-moving wave fronts collide and then either pass through or annihilate each other, depending on which sublattice they occupy. If the initially entangled sites are on different sublattices, then according to Eq. 3.21 all of the fermion operators $c_j(t)$ that contribute to the time evolution of the system will have odd indices for one wave and even indices for the other. Therefore, in this case the time evolution of

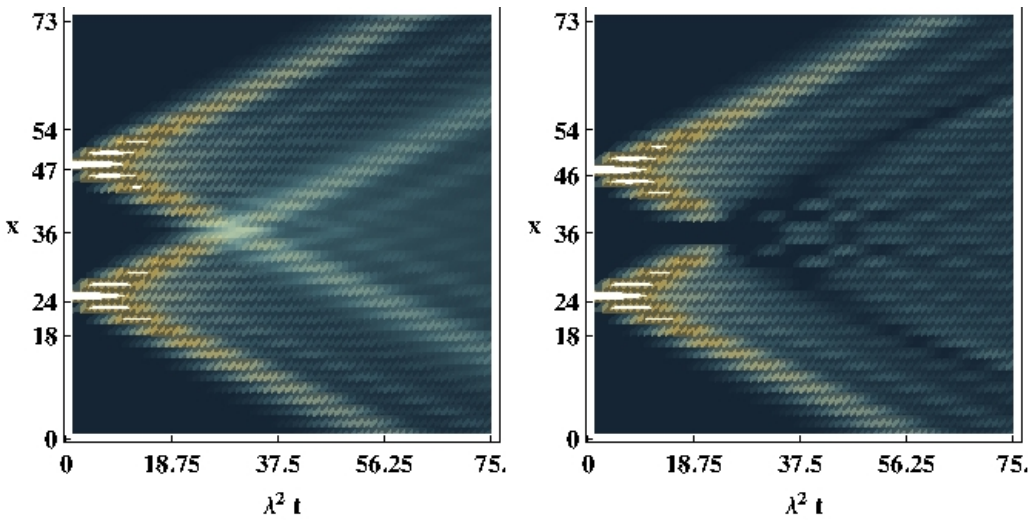

Figure 3.11: Time evolution of $C_{i,i+2}$ for $\lambda = 0.05$ and $\gamma = 0$. The two initially entangled pairs or sites in the left figure are on different sublattices. In the right figure the two pairs are on the same sublattice.

the two colliding waves proceeds independently. If on the other hand, the two waves are on the same sublattice, Eq. 3.21 may again be used to show that, when the waves intersect, all the entanglement they were transmitting is exactly negated by the other wave. This negative interference is a generic property of the uniform field models, where it can present a serious problem for a simultaneous unimpeded propagation of multiple flying qubits.

As λ is increased the term in Eq. 3.21 proportional to the function $\beta_j(t)$ serves not only to dampen the transmission as already mentioned, but also to diminish the degree to which the waves confined to different sublattices maintain their integrity. Formally, this occurs due to the function $\beta_j(t)$ taking a nonzero value for all values of j, which allows for the two waves to mix, resulting in their loss of coherence.

The observed nearly exact cancellation of the transmitted concurrence is not a general result, since it occurs only when the two colliding waves are created at precisely the same time on the same sublattice. However, the ability of entanglement waves to pass through each other if they propagate on different sublattices is independent of the strength of the entanglement carried in each wave and also of the actual state that is transported.

3.4.4 Effect Of Anisotropy

The entanglement transmission of the staggered field XY model favors a $\gamma \ll 1$ in the isotropic case. By breaking either the XY or Ising symmetry, the ground state of the system moves even further away from the Néel state, which has the effect of introducing even more vacuum excitations in the initial state. The net effect is that the quality of the entanglement transmission through the chain is degraded. Even so, it is interesting to study how this happens, and this effect is the subject of this section.

For both $\gamma \ll 1$, the fermion dispersion becomes $\omega_k = 1 - \gamma\lambda\cos(k) + \frac{\lambda^2}{2}\sin^2(k) + O(\lambda^3)$. The presence of mixed cosine and sine terms in the dispersion does not allow for a closed form for the function $\alpha_j(t)$ in Eq. 3.21 unless γ is also asymptotic. If $\lambda \gg \gamma$ the momentum sum over k in Eq. 3.21 may be integrated as before, and Eq. 3.22 still holds. In the opposite limit $\lambda \ll \gamma$, $\beta_j(t)$ is again negligible but the integration over k gives the new result

$$\alpha_j(t) \approx i^j J_j(\gamma\lambda t). \tag{3.29}$$

Here, the initial excitation is no longer confined to its own sublattice but propagates over the full lattice, the corresponding wavefront traveling with the speed $\sim \gamma\lambda$.

The intermediate regime $\lambda \sim \gamma \ll 1$ is presented in Fig. 3.12 where the nearest-sublattice-neighbor concurrence is plotted for only one side of the propagating wave in the case of $\lambda = 0.05$ and varying γ. Figure 3.12(a) is the isotropic case, with the entanglement confined to a single sublattice. For increasing anisotropy in Fig. 3.12(b) ($\gamma = 0.005$), 3.12(c) ($\gamma = 0.01$) and 3.12(d) ($\gamma = 0.02$) these two modes become apparent. The leading edge of the combined wavefront shows the emergence of an Ising-like wavefront, followed by the trailing isotropic component. Concomitant with the anisotropy, there is an increasing transfer of spectral weight from the latter to the former mode, which starts to dominate the transport of entanglement already at $\gamma\ \lambda$ and continues all the way to the Ising limit.

The decoherence profile is shown in Fig. 3.13 for both systems near the isotropic limit and the Ising limit. The Ising limit is not affected by a small degree of anisotropy, because until $\gamma \sim \lambda$ the dynamics of the system are governed by Eq. 3.29. Thus, for

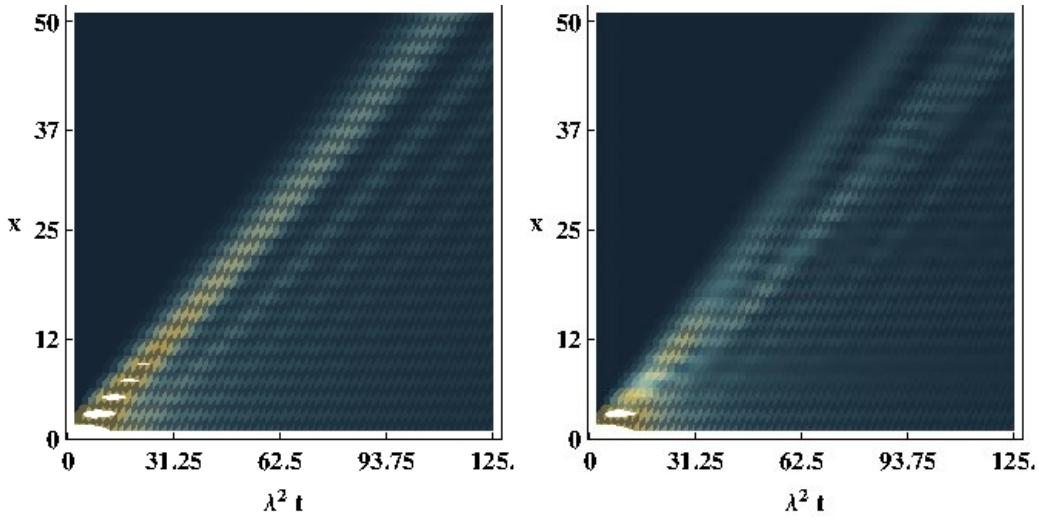

(a) $\gamma = 0$

(b) $\gamma = 0.005$

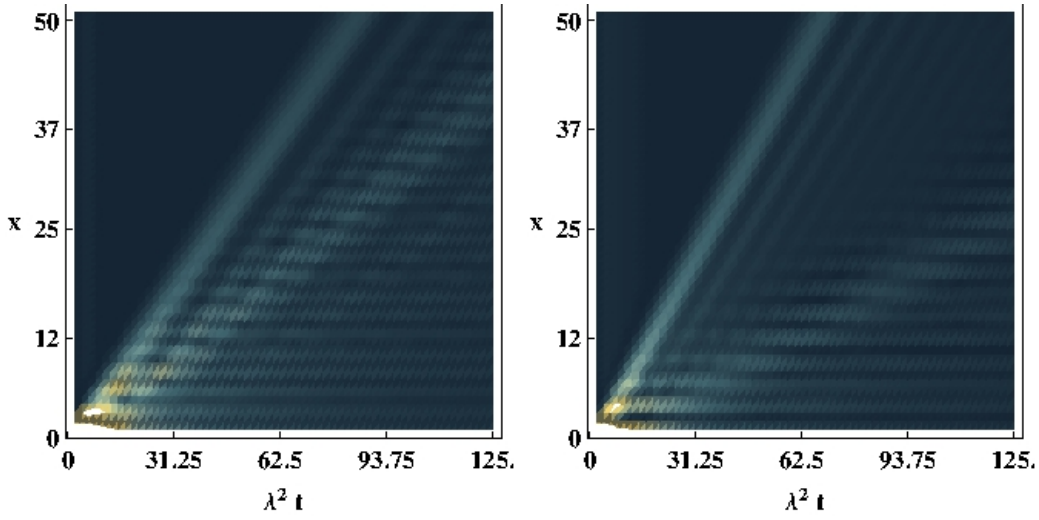

(c) $\gamma = 0.01$

(d) $\gamma = 0.02$

Figure 3.12: Time evolution of the concurrence $C_{i,i+2}$ for the anisotropic XY system in a staggered field, $\lambda = 0.05$.

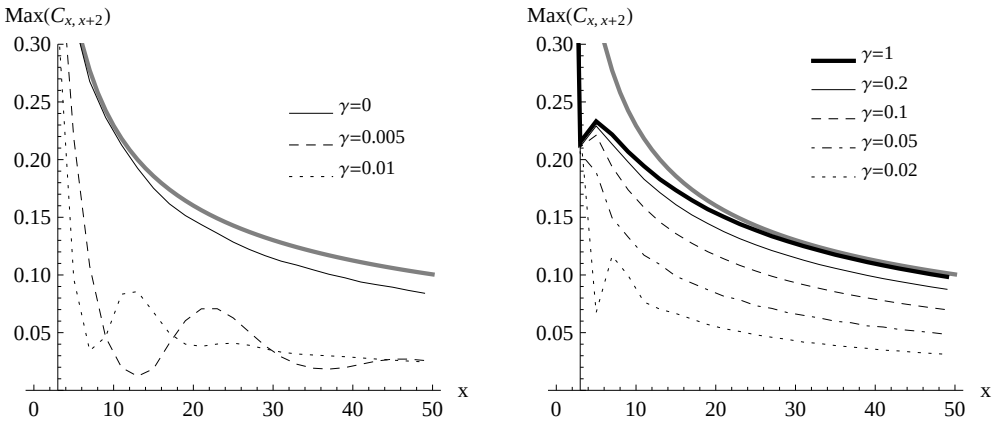

(a) Anisotropic XY

(b) Anisotropic Ising

Figure 3.13: Maximal concurrence $Max(C_{i,i+2})$ for the anisotropic XY system near the isotropic and Ising limits for $\lambda = 0.05$. The gray line represents $C_{x,x+2} = x^{1-\eta}$ for $\eta = 3/2$.

$\lambda = 0.05$ it is only at $\gamma \sim 0.2$ until there is a departure from the entanglement transmission characteristics of the Ising case. On the other hand, the isotropic model is much more sensitive to anisotropic effects in the small γ limit, as seen in Fig. 3.13(a). Once the $U(1)$ symmetry is broken the entanglement transfer characteristics of the chain diminish dramatically as the curves for $\gamma = 0.005$ and $\gamma = 0.01$ demonstrate. Of incidental interest in these graphs is that as $x- > \infty$ the entanglement achieves an small asymptotic value. This effect is due to vacuum fluctuations that give rise to entangled states even in the absence of an initially unentangled chain.

Chapter 4

Josephson Junctions

The remainder of this work is primarily concerned with the subject of Josephson junctions. A Josephson Junction is formed when two superconducting materials are placed in close proximity to one another. The the electrons in the bulk material have a wavefunction that extends beyond the boundary of the material, which in general is function of the normal distance r from the material, proportional to $e^{-\alpha r}$ for some material-dependent $\alpha > 0$. If the wavefunctions of the electrons in the two superconductors have a significant overlap then there is a finite chance for electrons to tunnel between the superconductors.

4.1 Introduction To Josephson Junctions

The simplest model for a Josephson junction consists of two identical superconducting leads separated by narrow gap filled with an insulating material. In this simplest case, the leads themselves are large, so that coulomb blockade effects may be ignored. That is, it requires negligible energy for a lead to accept another electron. For now it is assumed that the properties of the superconductors, namely the order parameter, are isotropic (s-wave). Josephson [73] first studied this system and predicted the time dependence of the supercurrent across the junction as a function of the potential difference of the two superconducting leads.

The wave function for an electron on one of the leads may be written as

$$\psi_{L,R} = \sqrt{\rho_{L,R}} e^{i\theta}, \tag{4.1}$$

where ρ is the electron density. If a potential V is imposed across the leads which are coupled with a strength K, the Schrodinger equation reads

$$\begin{aligned} i\frac{\partial \psi_L}{\partial t} &= eV\psi_L + K\psi_R \\ i\frac{\partial \psi_R}{\partial t} &= -eV\psi_R + K\psi_L. \end{aligned} \tag{4.2}$$

The solution of this system is found by equating real and imaginary parts. Writing $\theta_{RL} = \theta_R - \theta_L$,

$$\begin{aligned} \frac{\partial \rho_L}{\partial t} &= 2K\sqrt{\rho_L \rho_R}\sin(\theta_{RL}) \\ \frac{\partial \rho_R}{\partial t} &= 2K\sqrt{\rho_R \rho_L}\sin(\theta_{LR}) \\ \frac{\theta_L}{\partial t} &= K\sqrt{\frac{\rho_R}{\rho_L}}\cos(\theta_{RL}) - eV \\ \frac{\theta_R}{\partial t} &= K\sqrt{\frac{\rho_L}{\rho_R}}\cos(\theta_{RL}) + eV. \end{aligned} \tag{4.3}$$

The first two equations describe how the electron densities would begin to change in the absence of any outside force to restore them. However ρ_L and ρ_R do not change since the left and right leads are both connected to the battery holding them at a fixed voltage. What the first two equations describe then is the current density through the junction, or

$$J = 2K\rho\sin(\theta_{RL}(t)). \tag{4.4}$$

This current density is more commonly expressed as a current $I = I_0\sin(\theta_{RL})$ where I_0, the critical current, is a function of the area and spacing of the tunnel junction as well as the characteristics of the superconductor. The second two equations give

$$\theta_{RL}(t) = \theta_{RL}(0) + 2e\int V(t)dt. \tag{4.5}$$

So if V(t)=0, there is a constant supercurrent across the junction, a phenomena known as the *DC Josephson Effect*. On the other hand, a non-zero constant voltage causes a oscillatory current across the junction and is *AC Josephson Effect*, however clearly the DC effect is just the $\omega \to 0$ case of the AC effect.

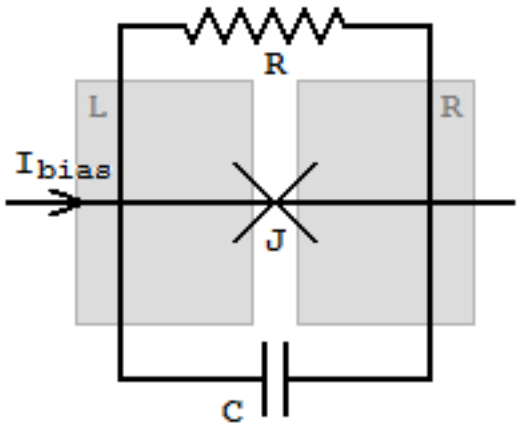

Figure 4.1: Circuit representation of a resistively shunted Josephson junction

4.1.1 Josephson Qubits

A quantum spin with moment μ in a magnetic field $B\hat{z}$ has two possible eigenstates: either aligned with the field, in which case the energy of the state is $-\mu B$ or anti-aligned, with energy $+\mu B$. It is a true two level quantum system as there are no other eigenstates but the particle itself can be in a superposition of these two states. Josephson junctions may also be configured to behave as a two levels system, and this can be done in a variety of ways.

If the electrical capacitance of the leads is small then Coulomb Blockade effects become important, and it is possible to control the number of Cooper-pair charges on each grain. If immersed in an electric field, then one can build a two level system with the ground state energy $E_0 = eE(N_R - N_L)$ and first excited state energy $E_1 = E_0 + 2eE$. This configuration where the states of the two level system are determined by the charge difference across the junction is called a *charge qubit* [13].

Another type of qubit requiring Josephson junctions to operate is called the *flux qubit*, and is essentially a SQUID or Superconducting Quantum Interference Device. The current in a loop travels in one direction for half-integer multiples of magnetic field flux quanta inside the loop, and the other direction for integral multiples of flux [14].

The third type of commonly mentioned Josephson qubit is the *phase qubit*. While a physical realization of a phase qubit requires several junctions [15], its behavior can be studied by considering a capacitative and resistive shunted Josephson junction, Fig.

4.1. The resistor represents a dissipative electron transfer from one lead to the other though the intervening medium and the shunting capacitor is simply the capacitance of the Josephson junction. When in operation a bias current I_{bias} is maintained across the junction. Conservation of current yields the dynamical equation for the phase

$$I_{bias} = I_0 \sin(\theta_{RL}) + \frac{1}{2eR}\frac{\partial \theta_{RL}}{\partial t} + \frac{C}{2e}\frac{\partial^2 \theta_{RL}}{\partial^2 t}. \tag{4.6}$$

This equation of motion describes particle of mass $\sim C$ moving in θ_{RL} space with a frictional coefficient $\sim 1/R$, subject to a potential $V = -I_{bias}(\theta_{RL} + \frac{I_0}{I_{bias}}\cos(\theta_{RL}))$. If $I_{bias} \ll I_0$ then the potential the particle experiences is a washboard potential with periodic metastable states every 2π in θ_{RL}. To produce a qubit capable of readout, the bias current is so that only 3 bound states exist (see Fig. 4.2). A particle in states $|0\rangle$ or $|1\rangle$ are meta-stable and have a small tunneling transmission amplitude. State $|2\rangle$ on the other hand, is tuned so that it decays almost immediately.

In a phase qubit, states $|0\rangle$ or $|1\rangle$ form the required two level system. In order to read the value of the qubit, the current is perturbed by $\omega_{2,1}$, which results in a particle in state $|0\rangle$ transitioning to the metastable state $|1\rangle$, but $|1\rangle \rightarrow |2\rangle$, which tunnels a short time later, resulting in a perceptible current.

Each of these three schemes for manufacturing a qubit out of Josephson junctions, but for the present work, the phase qubit is the most interesting. One can imagine a chain of these Josephson junctions with a bias current going through each of them sequentially. This configuration bears a similarity to a quantum spin 1/2 chain, in that both are chains of sequential two level systems. A minor difference is that the state of a qubit in the Josephson chain is dependent on the phase difference $\theta_{i,i+1}$ of the two islands at sites i and $i+1$ and thus is established *on-link* versus *on-site* for the chain.

In a dissipative periodic system such as this, the effect of dissipation is to reduce the probability that the particle tunnels to the next meta-stable state [74]. This competes with the critical current I_0, which governs the depth of the meta-stable well, so that for a large I_0 the probability of the system to tunnel to an adjacent metastable phase is further reduced. This state where the phase is locked in is reminiscent of the

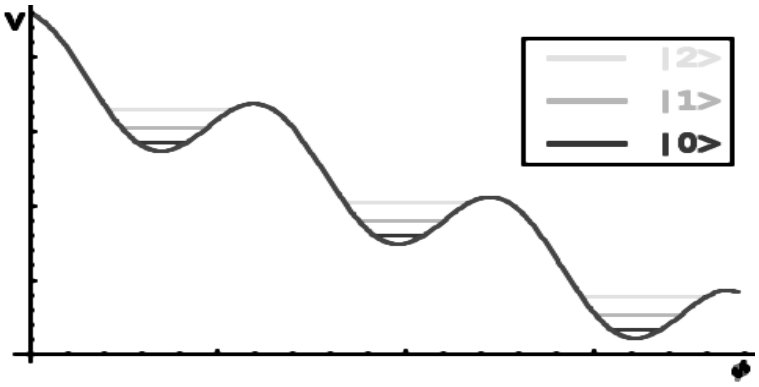

Figure 4.2: The 'Washboard' potential of a current-biased resistively shunted Josephson junction

the small λ state of the quantum spin chain, where the spins tend to align with the applied field - and also where the highest fidelity entanglement transfer is possible. The ground state phase diagram for a network of (conventional) superconductors has been found[23], and this state where the phase is locked corresponds, in general, to the collective superconducting state of the entire network. For a large dissipation and small Josephson coupling, the system is in a resistive (metallic) state, and is both parameters are small the system is insulating. The on-link phase and charge difference are dual to each other, so for a mobile phase, the charges in the network are locked, and for a locked phase the charges are highly mobile.

This discussion may be extended to superconductors that do not display isotropic (s-wave) characteristics. The next section addresses this, with the goal being to determine the ground state phase diagram and electrical conductivity of a network of superconductor islands that possess d-wave symmetry[75].

4.2 Josephson Junction Arrays

The analysis of a Josephson junction array begins by writing the effective action $S = S_C + S_T$ where

$$S_C = \int_0^{1/T} d\tau \frac{1}{2}[\sum_i C_{ii}(\frac{\partial\phi_i(\tau)}{\partial\tau})^2 + \sum_{\langle i,j\rangle} C_{ij}(\frac{\partial\phi_{ij}(\tau)}{\partial\tau})^2]$$

$$
\begin{aligned}
S_T &= -\sum_{\langle i,j\rangle}\int_0^{1/T} d\tau \int_0^{1/T} d\tau' \alpha(\tau-\tau')\cos(\phi_{ij}(\tau)-\phi_{ij}(\tau')) \\
&- \sum_{\langle i,j\rangle}\int_0^{1/T} d\tau \int_0^{1/T} d\tau' \beta(\tau-\tau')\cos(\phi_{ij}(\tau)+\phi_{ij}(\tau')).
\end{aligned} \tag{4.7}
$$

This is an extension of the effective action for a single junction [76], whose derivation from the microscopic BCS Hamiltonian is presented in Appendix A. In this equation S_C is the part of the action due to both the self and inter-grain capacitances, C_{ij} denotes the inter-grain capacitance or, in the case where $i = j$ the self-capacitance. Also, ϕ_i is the phase of the superconducting order parameter Δ_i and the difference in phases on two sites i and j is $\phi_{ij} = \phi_i - \phi_j$.

The part of the action that describes tunneling is S_T and accounts for two different types of processes. The α-term describes dissipation due to the Andreev quasiparticle tunneling whose effects have been extensively discussed in the previous works [23], while the β-term represents the processes of (in general, non-synchronous) pair tunneling. To leading order in the tunneling matrix element $T(k,k')$ the tunneling kernels $\alpha(\tau)$ and $\beta(\tau)$ are

$$
\begin{pmatrix}\alpha(\tau)\\ \beta(\tau)\end{pmatrix} = -2\int \frac{d^Dk}{(2\pi)^D}\frac{d^Dk'}{(2\pi)^D}\,|\mathrm{T}(k,k')|^2 \begin{pmatrix} G_L(k,\tau)G_R(k',-\tau)\\ F_L(k,\tau)F_R(k',-\tau)\end{pmatrix}, \tag{4.8}
$$

where $G(k,i\omega_n) = \frac{i\omega_n+\xi_k}{\omega_n^2+\xi_k^2+\Delta_k^2}$ and $F(k,i\omega_n) = \frac{\Delta_k}{\omega_n^2+\xi_k^2+\Delta_k^2}$ are the normal and anomalous electron Green functions respectively.

In the conventional (s-wave) superconductors the tunneling amplitude is independent of momentum and $\alpha(\tau) \propto 1/\tau^2$. The pair tunneling kernel $\beta(\tau) \propto e^{-\Lambda|\tau|}$, which strongly suppresses contributions where $\tau \neq \tau'$ thereby reducing the last term in Eq. 4.7 to a single time integral $E_J\int_0^{1/T} d\tau \cos 2\phi_{ij}(\tau)$ which is identified as the local Josephson energy $E_J = \int_0^{1/T} d\tau\beta(\tau)$.

In the case of a gapless superconductor one obtains strongly retarded kernels

$$
\alpha(\tau)/\alpha = \beta(\tau)/\beta = 1/\tau^{2D-\eta}, \tag{4.9}
$$

where the prefactor in the β kernel vanishes for any factorizable matrix element, $T(k,k') = f(k)f(k')$, if the symmetry of the function $f(k)$ under the lattice group is

different from that of the gap Δ_k. Nonetheless, one can obtain a non-trivial result for $\beta(\tau)$ in the presence of a non-factorizable term $T(k,k') = g(k-k')$, the exponent η being its scaling dimension $g(\lambda \mathbf{q}) = g(\mathbf{q})/\lambda^{\eta}$.

A momentum conserving matrix element $T(k,k') = \delta(\vec{k} - \vec{k}')$ results in a solution for β for $D = 2$ with both tunneling kernels $\propto 1/\tau^2$ [28, 30]. A short-time divergence of Eqs.(3) can be naturally regularized by substituting $\tau \to \sqrt{\tau^2 + \Lambda^{-2}}$ where the cutoff scale Λ is set by the maximal superconducting gap in the bulk. It is worth mentioning that conceivably, one can encounter even longer-ranged correlations ($2D - \eta < 2$) in the presence of, e.g., resonant tunneling through zero energy states supported by certain tunneling configurations, such as that of the $d_0/d_{\pi/4}$ in-plane grain boundary [77, 78, 79].

4.2.1 Green Functions

Turning now to the effective action Eq. 4.7, the strongly retarded nature of the tunneling terms renders a customary dual representation based on the Villain transformation of the local Josephson term inapplicable, thereby making this model unsuitable for the standard mapping onto an effective vortex plasma [23]. Therefore, a well-known description of the different phases in terms of bound vortex-antivortex complexes (dipoles, quadrupoles, etc.) can not be readily generalized to the problem at hand, either, thus forcing one to take a different approach. To that end, a new bosonic field $\psi_i(\tau)$ is introduced, alongside an associated Lagrange multiplier field λ_i enforcing the local constraint $\psi_i(\tau) = e^{i\phi_i(\tau)}$.

This approach should be contrasted with the previously developed treatments of the conventional (local) Josephson term (see, e.g., Ref.[80, 81, 82]) where a constrained bosonic variable would be used to represent the pair field $e^{2i\phi_i(\tau)}$. Indeed, an attempt to implement this technique in the present (non-local) case would require one to work with a technically intractable bi-local composite operator $\psi_i(\tau)\psi_i(\tau')$.

By integrating out the phase variable ϕ_i, keeping the leading terms of the corresponding cluster expansion (cf. with Ref.[80, 81, 82]), and then integrating out the

Lagrange multiplier field, one arrives at the partition function (see Appendix B)

$$\begin{aligned} Z &= \int D\psi_i^\dagger(\tau) D\psi_i(\tau) D\lambda_i(\tau) \exp(-S_{eff}) \\ S_{eff} &= \sum_{\langle i,j \rangle} \int_0^{1/T} d\tau_1 \int_0^{1/T} d\tau_2 \psi_i^\dagger(\tau_1) [W_{ij}^{-1}(\tau_1 - \tau_2) \\ &+ \delta_{ij} \lambda_i(\tau_1) \delta(\tau_1 - \tau_2)] \psi_j(\tau_2) \\ &+ \alpha(\tau_1 - \tau_2) \psi_i^\dagger(\tau_1) \psi_j^\dagger(\tau_2) \psi_i(\tau_2) \psi_j(\tau_1) \\ &+ \beta(\tau_1 - \tau_2) \psi_i^\dagger(\tau_1) \psi_i^\dagger(\tau_2) \psi_j(\tau_2) \psi_j(\tau_1) + h.c.)]), \end{aligned} \tag{4.10}$$

where $\lambda_i(\tau)$ is an additional Lagrange multiplier enforcing the auxiliary constraint $\psi_i^\dagger(\tau)\psi_i(\tau) = 1$ which is not automatically satisfied unless the integration over $\phi_i(\tau)$ is performed exactly.

The correlation function appearing in Eq. 4.10,

$$\begin{aligned} W_{ij}(\tau) = \left\langle e^{i\phi_i(\tau)} e^{-i\phi_j(0)} \right\rangle = \\ \exp[-\int \frac{d\omega d^D k}{(2\pi)^{D+1}} \frac{1 - \cos(\omega\tau - \vec{k}\,(\vec{r}_i - \vec{r}_j))}{\omega^2 C(k)}] = \delta_{ij} e^{-E_C|\tau|} \end{aligned} \tag{4.11}$$

is governed by the effective Coulomb energy $E_C = \int \frac{d^D k}{2(2\pi)^{D+1} C_k}$ proportional to the integral of the inverse capacitance $C_k = \sum_{\langle i,j \rangle} C_{ij} e^{i\vec{k}(\vec{r}_i - \vec{r}_j)}$ which converges, provided that the capacitance matrix progressively decreases with the separation between the sites.

The frequency integral in Eq. 4.11 diverges for any $\vec{R}_{ij} \neq 0$ which dictates that the correlation function $W_{ij}(\tau)$ remains strictly local in the real space. Also, Eq. 4.11 is written in the limit of vanishing temperature, while at finite T a proper account of large phase fluctuations with non-trivial winding numbers makes this (as well as any bosonic) function periodic with a period $1/T$ by virtue of the substitution $\tau \to \tau - T\tau^2$ (see Ref.[23]).

At $\alpha = \beta = 0$ one then obtains a bare (normal) Green function

$$G_{ij}^{(0)}(\omega) = \frac{2\delta_{ij}}{\omega^2/E_C + E_C}, \tag{4.12}$$

while for finite α and β the quantum charge fluctuations give rise to the corrections which can be incorporated into the normal $G_{ij} = \left\langle \psi_i \psi_j^\dagger \right\rangle$ and anomalous $F_{ij} = \langle \psi_i \psi_j \rangle$ Green functions obeying the usual Dyson's equations (see Appendix C)

$$\begin{pmatrix} G_{ij} \\ F_{ij} \end{pmatrix} = \begin{pmatrix} G_{ij}^{(0)} \\ 0 \end{pmatrix} + G_{ik}^{(0)} \sum_{kl} \begin{pmatrix} \Sigma_{kl} & \Delta_{kl} \\ \Delta_{kl} & \Sigma_{kl} \end{pmatrix} \begin{pmatrix} G_{lj} \\ F_{lj} \end{pmatrix}, \tag{4.13}$$

where both the normal Σ_{ij} and anomalous Δ_{ij} self-energies can be computed as series expansions in powers of α and β.

The analysis of these expansions shows that they can be organized according to the powers of the inverse coordination number z (e.g., $z = 2D$ for a simple cubic lattice). In the leading approximation for $z \gg 1$, the self-energies are given by the equations

$$\begin{aligned} \Sigma_{ij}(\omega) &= \int \frac{d\omega'}{2\pi} [\delta_{ij} \sum_l \alpha(\omega - \omega') G_{ll}(\omega') + (\alpha(0) + \beta(0) + \beta(\omega - \omega')) G_{ij}(\omega')] \\ \Delta_{ij}(\omega) &= \int \frac{d\omega'}{2\pi} [\alpha(\omega - \omega') F_{ij}(\omega') + \delta_{ij} \sum_l \beta(\omega - \omega') F_{ll}(\omega')]. \end{aligned} \tag{4.14}$$

When ascertaining a general layout of the phase diagram of the Josephson junction array, different components of the self-energy can serve as emergent order parameters. As such, one can distinguish between the local, $\Sigma_0 = \Sigma_{ii}$, and non-local, $\Sigma_1 = \frac{1}{z} \sum_\mu \Sigma_{i,i+\mu}$ (here the sum is taken over the z nearest neighbors), normal, as well the corresponding anomalous, $\Delta_0 = \Delta_{ii}$ and $\Delta_1 = \frac{1}{z} \sum_\mu \Delta_{i,i+\mu}$, self-energies.

Specifically, Σ_1 signals the onset of a metallic behavior (hopping between neighboring sites), Δ_0 manifests an incipient local pairing, Δ_1 serves as the precursor of superconducting coherence setting in across the entire Josephson junction network, while a frequency-dependent part of the Σ_0 indicates the development of local time correlations.

With the on-site and nearest-neighbor terms taken into account, the spatial Fourier harmonics read

$$\begin{pmatrix} \Sigma(\omega, k) \\ \Delta(\omega, k) \end{pmatrix} = \begin{pmatrix} \Sigma_0(\omega) \\ \Delta_0(\omega) \end{pmatrix} + \begin{pmatrix} \Sigma_1(\omega) \\ \Delta_1(\omega) \end{pmatrix} \gamma(k) + ... \tag{4.15}$$

where $\gamma(k) = \sum_\mu e^{ik\mu}$.

Equations 4.14 can be further improved by adding polarization corrections to the effective coupling terms (see Appendix D)

$$\begin{pmatrix} \tilde{\alpha} \\ \tilde{\beta} \end{pmatrix} = \begin{pmatrix} \alpha \\ \beta \end{pmatrix} + \begin{pmatrix} \Pi_E & \Pi_O \\ \Pi_O & \Pi_E \end{pmatrix} \begin{pmatrix} \alpha & \beta \\ \beta & \alpha \end{pmatrix} \begin{pmatrix} \tilde{\alpha} \\ \tilde{\beta} \end{pmatrix}, \tag{4.16}$$

where the polarization functions $\Pi_{E,O}(\omega) = \int \frac{d\omega'}{2\pi} \Gamma_{E,O} G(\omega') G(\omega - \omega')$ include the vertex corrections $\Gamma_{E,O}$ arising from the even and odd numbers of non-crossing β-couplings

$$\begin{pmatrix} \Gamma_E \\ \Gamma_O \end{pmatrix} = \begin{pmatrix} 1 \\ \beta \end{pmatrix} + \begin{pmatrix} \beta^2 & 0 \\ 0 & \beta^2 \end{pmatrix} \begin{pmatrix} \Gamma_E \\ \Gamma_O \end{pmatrix}. \tag{4.17}$$

With the vertex and polarization corrections included and in the absence of any emergent order parameters, the self-consistent equation for $\Sigma_0(\omega)$ reads

$$\Sigma_0(\omega) = z \int \frac{d\omega'}{2\pi} \bar{\Gamma}(\omega') \frac{\tilde{\alpha}(\omega - \omega')}{G_0^{-1}(\omega') - \Sigma_0(\omega')}. \tag{4.18}$$

The (static and spatially uniform) expectation value of the Lagrange multiplier $\lambda = \langle \lambda_i(\tau) \rangle$ can then be determined from the normalization condition $\int \frac{d\omega d^D k}{(2\pi)^{D+1}} G(\omega, k) = 1$.

4.2.2 Conductivity Phase Diagram

In order to ascertain the locations of the putative phase boundaries a constant term $\Sigma_0(0) + \lambda$ is included into the definition of the renormalized Coulomb energy $\tilde{E}_c$ and expand Eq. 4.14 to the first order in the emergent self-energies Σ_1, Δ_0, Δ_1, as well as the derivative of the (linear) frequency-dependent part of $\Sigma_0(\omega)$.

Threshold values of the couplings, beyond which such self-energy components develop, are then given by the eigenvalue equations

$$\begin{aligned}
\Sigma_1(\omega) &= \int \frac{d\omega'}{2\pi} \Gamma [\tilde{\alpha}(0) + \tilde{\beta}(0) + \tilde{\beta}(\omega - \omega')] G_0^2(\omega') \Sigma_1(\omega') \\
\Delta_0(\omega) &= z \int \frac{d\omega'}{2\pi} \Gamma \tilde{\beta}(\omega - \omega') G_0^2(\omega') \Delta_0(\omega') \\
\Delta_1(\omega) &= \int \frac{d\omega'}{2\pi} \Gamma \tilde{\alpha}(\omega - \omega') G_0^2(\omega') \Delta_1(\omega') \\
\frac{d\Sigma_0(\omega)}{d\omega} &= z \int \frac{d\omega'}{2\pi} \Gamma \tilde{\alpha}(\omega') G_0^2(\omega') \frac{d\Sigma_0(\omega')}{d\omega'}.
\end{aligned} \tag{4.19}$$

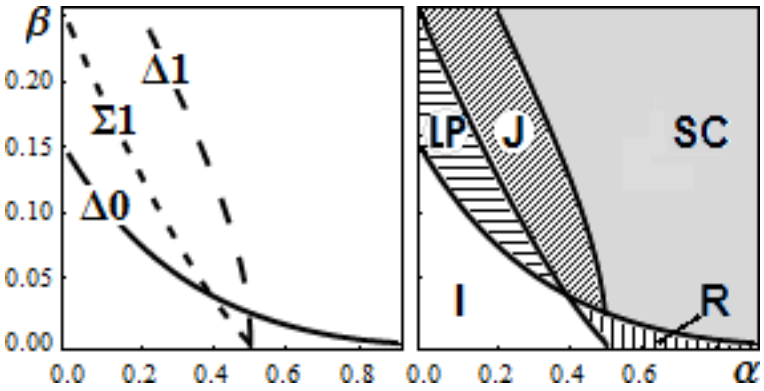

Figure 4.3: Left panel: The onset of the inter-site self energy Σ_1 and both on-site and inter-site anomalous self energies Δ_0 and Δ_1. Right panel: phase diagram (see text)

In the case of marginal ('Ohmic') dissipation corresponding to $2D - \eta = 2$ the Fourier transforms of the (regularized) coupling functions behave as $\alpha(\omega)/\alpha = \beta(\omega)/\beta = \pi\Lambda e^{-|\omega|/\Lambda}$, thus resulting in only a weak frequency dependence of the self-energy at $\omega \ll \Lambda$.

The first three of the eigenvalue equations (Eq. 4.19) then reduce to the algebraic ones

$$\begin{aligned} 1 &= (\Gamma_E^2 + \Gamma_O^2)(2\tilde{\beta} + \tilde{\alpha}) + 2\Gamma_E\Gamma_O(2\tilde{\alpha} + \tilde{\beta}) \\ 1 &= z\left(\Gamma_E^2\tilde{\beta} + 2\Gamma_E\Gamma_O\tilde{\alpha} + \Gamma_O^2\tilde{\beta}\right) \\ 1 &= \Gamma_E^2\tilde{\alpha} + \Gamma_O^2\tilde{\alpha} + 2\Gamma_E\Gamma_O\tilde{\beta}, \end{aligned} \tag{4.20}$$

from which one determines the locations of the putative critical lines in the $\alpha - \beta$ plane (see Fig. 4.3).

Interestingly enough, Eqs. 4.20 suggest that for small α and large z the onset of local ('on-site') pairing upon increasing β may precede that of the metallic behavior, while for small β the inter-site ('bond') pairing emerges only at sufficiently large α.

The above observations suggest a general layout of the phase diagram presented in Fig. 4.3. The region of small α and β with $\Sigma_1 = \Delta_0 = \Delta_1 = 0$ is interpreted as uniformly insulating (I), while the emergent order parameter $\Delta_0 \neq 0$ signals the onset of local superconducting pairing (LP) at $\beta \sim 1/z$. At still higher values of $\beta \sim 1$ one expects to enter a Josephson-like phase (J) with $\Delta_0, \Sigma_1 \neq 0$ but without global coherence. On the other hand, at $\alpha \sim 1$ the insulator gives way to the resistive

phase (R) with $\Sigma_1, \Delta_1 \neq 0$ which supports both, Cooper pair and single quasiparticle, transport.

Lastly, the uniformly superconducting phase (SC) with $\Sigma_1, \Delta_{0,1} \neq 0$ would eventually be attained at $\alpha, \beta \gtrsim 1$. It should be noted, though, that these predictions are based on the approximate perturbative analysis and, therefore, not all the putative phase boundaries may actually be present in the real system. In particular, there may or may not be a physical distinction other than a crossover between the J and LP phases, or the latter regime might be absent altogether (as it is for $z = 2$).

Such caveats notwithstanding, the overall behavior appears to be somewhat reminiscent of that in the standard (s-wave) case: the system can be nudged closer to the superconducting state by increasing either, the Cooper pair or particle-hole tunneling, the latter providing a mechanism for intrinsic dissipation which quenches phase fluctuations and promotes the classical Josephson effect.

Should, however, the tunneling β-term happen to decay even more slowly ($2D-\eta < 1$), the analog of the effective Josephson energy would then diverge at large τ, thus making the infrared behavior essentially singular and possibly allowing for some drastic changes in the phase structure.

4.2.3 Calculation Of Conductivity

The electrical conductivity of the Josephson junction array may be computed by considering the liner response of the system to an electromagnetic perturbation [83]. An external vector potential A_μ is introduced into the action (Eq. 4.7) which amounts to a substitution $\nabla_\mu \phi_i(\tau) \to \nabla_\mu \phi_i(\tau) + A_\mu(\tau)$. Formally, the conductivity is given by the Kubo formula

$$\sigma_{i,xy}(\omega) = -\frac{1}{\omega_m} \, J_{i,xy}(\omega)|_{i\omega_m \to \omega + i0} \tag{4.21}$$

where

$$J_{i,xy}(\tau_1, \tau_2) = Z^{-1} \frac{\partial^2}{\partial A_{i,x}(\tau_1) \partial A_{i,y}(\tau_2)} Z\,[A]\Big|_{A=0} \tag{4.22}$$

and here $Z = \mathrm{Tr}\exp[-S[A]]$ where $S[A]$ is the action (Eq. 4.7) with the vector potential substitution. The electrical conductivity is therefore determined by the averages

$$\begin{aligned} J_{xy}(\tau,\tau') &= J_{xy,para}(\tau,\tau') + J_{xy,dia}(\tau,\tau') \\ J_{xy,dia} &= \left\langle \frac{\partial^2 S}{\partial A_x(\tau)\partial A_y(\tau')}\bigg|_{A=0} \right\rangle_S \\ J_{xy,para} &= \left\langle \frac{\partial S}{\partial A_x(\tau)}\frac{\partial S}{\partial A_y(\tau')}\bigg|_{A=0} \right\rangle_S , \end{aligned} \tag{4.23}$$

which take the intermediate form for the paramagnetic term,

$$\begin{aligned} &\left\langle \frac{\partial S}{\partial A_x(\tau_1)}\frac{\partial S}{\partial A_y(\tau_2)}\bigg|_{A=0} \right\rangle_S = \\ &= 2\int_0^{1/T} d\tau \left\langle (\alpha(\tau-\tau_2)\sin(\nabla_y\phi_i(\tau_2) - \nabla_y\phi_i(\tau))\right\rangle_S \\ &\qquad + \left\langle \beta(\tau-\tau_2)\sin(\nabla_y\phi_i(\tau_2) + \nabla_y\phi_i(\tau)))\right\rangle_S \\ &\times 2\int_0^{1/T} d\tau' \left\langle (\alpha(\tau'-\tau_1)\sin(\nabla_x\phi_i(\tau_1) - \nabla_x\phi_i(\tau'))\right\rangle_S \\ &\qquad + \left\langle \beta(\tau'-\tau_1)\sin(\nabla_x\phi_i(\tau_1) + \nabla_x\phi_i(\tau')))\right\rangle_S , \end{aligned} \tag{4.24}$$

and for the diamagnetic term,

$$\begin{aligned} &\left\langle \frac{\partial^2 S}{\partial A_x(\tau_1)\partial A_y(\tau_2)}\bigg|_{A=0} \right\rangle_S = \\ &= 2\delta_{xy}\delta_{\tau_1\tau_2}\left(\int_0^{1/T} d\tau'\alpha(\tau_1-\tau')\left\langle \cos(\nabla_x\phi_i(\tau_1) - \nabla_x\phi_i(\tau'))\right\rangle_S\right) \\ &\qquad -2\delta_{xy}\alpha(\tau_1-\tau_2)\left\langle \cos(\nabla_x\phi_i(\tau_1) - \nabla_x\phi_i(\tau_2))\right\rangle_S \\ &+2\delta_{xy}\delta_{\tau_1\tau_2}\left(\int_0^{1/T} d\tau'\beta(\tau_1-\tau')\left\langle \cos(\nabla_x\phi_i(\tau_1) + \nabla_x\phi_i(\tau'))\right\rangle_S\right) \\ &\qquad +2\delta_{xy}\beta(\tau_1-\tau_2)\left\langle \cos(\nabla_x\phi_i(\tau_1) + \nabla_x\phi_i(\tau_2))\right\rangle_S . \end{aligned} \tag{4.25}$$

It is evident that $J_{xy,para}$ will be second order in $\{\alpha,\beta\}$ so that for $\alpha,\beta \lesssim 1$ the dominant contribution comes from J_{dia}. To arrive at an expression for $\sigma(\omega)$ it is necessary to Fourier transform the above expression. Doing so yields

$$\sigma_{xy}(\omega) \quad = \delta_{xy} \quad \int_0^{1/T} d\tau \left[\alpha(\tau)\frac{1-e^{i\omega\tau}}{\omega}\left\langle \cos(\nabla_x\phi_i(0) - \nabla_y\phi_i(\tau))\right\rangle_S\right.$$

$$+ \qquad \beta(\tau)\frac{1+e^{i\omega\tau}}{\omega}\left\langle\cos(\nabla_x\phi_i(0)+\nabla_y\phi_i(\tau))\right\rangle_S\Bigg]. \tag{4.26}$$

The averages may be expanded to produce a form for the conductivity that has an explicit dependence on the regular and anomalous Green functions

$$\begin{aligned}\langle\cos(\nabla_x\phi_i(0)-\nabla_y\phi_i(\tau))\rangle &= \left\langle\psi_i^\dagger(0)\psi_{i+x}(0)\psi_i(\tau)\psi_{i+y}^\dagger(\tau)\right\rangle \\ &= \left\langle\psi_i^\dagger(0)\psi_{i+x}(0)\right\rangle\left\langle\psi_i(\tau)\psi_{i+y}^\dagger(\tau)\right\rangle \\ &+ \left\langle\psi_i^\dagger(0)\psi_i(\tau)\right\rangle\left\langle\psi_{i+x}(0)\psi_{i+y}^\dagger(\tau)\right\rangle \\ &+ \left\langle\psi_i^\dagger(0)\psi_{i+y}^\dagger(\tau)\right\rangle\langle\psi_{i+x}(0)\psi_i(\tau)\rangle \\ &= G_x^\dagger(0)G_y(0)+G_0^\dagger(\tau)G_{y-x}(\tau)+F_y^\dagger(\tau)F_{-x}(\tau). \end{aligned} \tag{4.27}$$

The β term for σ_{xy} is found in a similar manner. With these expansions, the longitudinal conductivity takes the form

$$\begin{aligned}\sigma_{xx}(\omega) &\approx \int_0^{1/T} d\tau(\alpha(\tau)\frac{1-e^{i\omega\tau}}{\omega}[G_1^2(0)+G_0^2(\tau)+F_1^2(\tau)] \\ &+ \beta(\tau)\frac{1+e^{i\omega\tau}}{\omega}[G_1^2(0)+G_1^2(\tau)+F_0^2(\tau)]) \end{aligned} \tag{4.28}$$

and, upon performing the frequency integrations, one obtains (see Appendix E)

$$\sigma_{xx}(\omega)\approx\alpha[\frac{E_C}{T}e^{-2E_C/T}(1+\frac{\Delta_1^2}{E_C^2})+\frac{\Sigma_1^2}{E_C^2}]+\beta\delta(\omega)\frac{\Sigma_1^2+\Delta_0^2}{E_C^2}. \tag{4.29}$$

The emergent metallicity order parameter Σ_1 promotes a metal-like (temperature-independent at $T\to 0$) conductivity, thereby distinguishing it from the activation-type behavior characteristic of the insulating regime. Interestingly enough, it also contributes to the superfluid density, alongside the local pairing Δ_0, while the non-local one (Δ_1) does not (to the lowest order in β).

It is conceivable, though, that there might be a (partial) cancellation between the 'diamagnetic' and 'paramagnetic' terms at $\alpha,\beta\sim 1$, as a result of which the conductivity could remain universal along the critical lines, akin to the situation in the conventional, s-wave, Josephson junction networks [84, 85, 86, 87] (it is worth reiterating that in the present case one can not readily invoke the charge-vortex duality on which the universality argument is based [23] due to the inapplicability of the underlying Villain transformation).

Chapter 5

Conclusion

The XY chain serves as convenient model to examine the dynamics of entanglement because it is a diagonalizable model for certain transverse field configurations. One such previously unexplored configuration, that where the transverse field has alternating sign for each spin site, is investigated in Chapter 3. This previously unexplored problem is of interest in those prospective designs of a quantum register where the local field can be created, for example, by a one dimensional antiferromagnetic crystal placed in the vicinity of the one dimensional qubit array.

The use of alternating fields in qubit chains might also be advantageous in light of their ability to create additional entanglement. Moreover, the study of various field configurations is important for optimizing (time-independent) local field profiles as a part of the general problem of finding the best parameter values for artificially engineered qubit chains (most notably, cold atoms in optical lattices or Josephson junctions arrays), as an alternative to the proposed use of time-dependent controls.

To that end, it is found that in the strong-field limit the system with a staggered field approaches the uniform field model in its ability to transport entanglement; however, the speed of state transfer appears to be lower. In this regime, the two sublattices of the chain act independently, so that the entanglement waves traveling on one sublattice will not interfere with those on the other one. Instead, the integrity of such waves remains largely intact, thereby facilitating the possibility of transporting multiple quantum bits at the same time. As the field weakens, the true ground state of

the staggered field system departs from the initial Néel-like state of the chain, and the resulting vacuum fluctuations degrade the entanglement transport capabilities of the chain.

The generally slow speed of transmission in the strong staggered field case increases the propagating states exposure to any environmental sources of decoherence, thus manifesting yet another potential trade-off which needs to be accounted for in the prospective designs of a practical one dimensional quantum register. This emergence of mutually contradicting criteria is not uncommon in the field of quantum computing in general, and in qubit-chain designs in particular.

The effect of anisotropy on the XY staggered field model was studied as well, and it was shown that the transmission starts to lose the characteristics of isotropic staggered field propagation for moderate values of the anisotropy parameter γ, as compared to the ratio λ between the exchange coupling and the magnetic field. As the staggered field chain only achieves high-fidelity transport for $\lambda \ll 1$, and maintains its characteristic transfer properties for $\gamma \ll \lambda$, any anisotropy (about the XX model) will in general result in a XY chain whose transport characteristics are considerably degraded. As the anisotropy increases, and the chain becomes more Ising-like the Ising transport characteristics are of course recovered.

In considering the XY chain, only uniform couplings in time and space and time-independent fields were considered. There has been some recent work in for staggered field chains where the sign of the couplings in the $\hat{x}$ and $\hat{y}$ directions is staggered as well [88]. The ground state magnetization and entanglement have been computed, but the problem of examining the entanglement dynamics of such a system remains unaddressed. In principle, the dynamics for such a system could be found using a technique similar to the one used in this work.

Additional recent interest in this field has focused on the effect that a time-varying magnetic field has on the ground state of the system. Specifically, when the magnetic field in the constant field XY model undergoes an adiabatic linear change from $+B$ to $-B$ in time τ (called a *quench*) for $B > J$ through a region of the phase diagram where the energy gap vanishes defects arise in the spin states. The rate of production

of defects can be quantified using the prediction of the Kibble-Zurek theory extended to quantum spin chains[89, 90]. For a uniform field XY chain with couplings the density of the kinks is found [46] to be $n_u = (2\pi\sqrt{\tau}\,|\gamma|)^{-1}$, which is in agreement with the $1/\sqrt{\tau}$ behavior predicted by Kibble-Zurek theory. This result can be extended to apply to the staggered field case by using the rotation in Eq. 3.15, so that

$$n_s = \frac{|\gamma|}{2\pi\sqrt{t}}. \tag{5.1}$$

It is also possible to perform a quench by allowing one or both of the couplings in $\hat{x}$ or $\hat{y}$ to vary with time. This has been examined in the uniform field case [46, 91], but remains to be considered in the staggered field configuration.

Another avenue of research which has received attention recently is the prospect of finding Majorana fermions at the ends of certain types of spin chains of finite length [92, 93]. Since the Majorana fermions generally are not directly coupled to the environment, it is proposed that an entangled pair of Majorana fermions might serve as a channel for quantum teleportation that is relatively free of decohering effects. These Majorana fermions are also thought to exist on the surfaces of topological superconductors and has resulted in a considerable amount of recent activity in this field [94, 95].

In Chapter 4 networks of two dimensional d-wave superconductors were considered, which if stacked along the c-axis and separated by insulators (topological superconductors) somewhat resemble the proposed spin chain systems where Majorana fermions are expected to exist. However, for problems of this type it is easier to work with the spin chains themselves, and lacking some experimental reason to consider this Josephson chain as either a conduit for entanglement or a environment for Majorana modes, interest has remained focused on spin models.

Instead, this work addresses a more basic question which is the determination of the phase diagram for a network of two dimensional d-wave superconductors, along with the electrical conductivity of such a system. The problem presents a new challenge by not being amenable to the customary approaches exploiting the intrinsic locality of the standard Josephson effective action [23]. By using an alternative representation, it

is found that the phase diagram of the system might feature the insulating, uniformly superconducting, Josephson (local pairing only), and metallic phases which can be identified by the corresponding emergent order parameters. The resultant phase diagram bears a similarity to that of a network of conventional superconductors, however it is conceivable that this picture might be further altered in the presence of resonant tunneling between zero energy states where the temporal decay of correlations can be even longer-ranged. It is hoped that this analysis will prompt a further investigation into (and provide an alternative means for interpreting the experimental data on) the assemblies of high-T_c Josephson junctions [96, 97] beyond the scope of the currently used phenomenological approach adapted from the earlier studies of the s-wave superconductors.

Appendix A

Derivation Of The Josephson Junction Action

It is not immediately obvious how the interaction terms in the action for the Josephson junction arise from the microscopic Hamiltonian of two coupled BCS superconductors, therefore a brief explanation of this calculation is warranted. A solution for the action describing the tunneling between two superconductors was first put forth by Ambegaokar, Eckern and Schon [76, 98] and the contents of this appendix is a summary of their method.

The BCS Hamiltonian for a D-dimensional superconductor is

$$\begin{aligned} H = &- \int d^D r \psi_\sigma^\dagger(r) \frac{1}{2m} \left(\nabla - ie\mathbf{A}\right)^2 \psi_\sigma(r) \\ &- \frac{g}{2} \int d^D r \psi_\sigma^\dagger(r) \psi_{-\sigma}^\dagger(r) \psi_{-\sigma}(r) \psi_\sigma(r) \\ &+ \int d^D r \frac{1}{8\pi} (h - h_{ext})^2. \end{aligned} \tag{A.1}$$

A summation over the spin is implied. A Josephson junction consists of two such superconductors, on either side of some insulating junction and denoted by the L and R for the left and right superconductor, respectively. In this configuration, the combined Hamiltonian of the system acquires new terms due to the tunneling electrons (H_T) and the charge difference across the junction (H_C) so that the full Hamiltonian is

$$H = H_L + H_R + H_T + H_Q \tag{A.2}$$

where

$$\begin{aligned} H_T &= \int_{r\in L} d^D r \int_{r'\in R} d^D r' \mathrm{T}(r,r')(\psi^\dagger_{L,\sigma}(r)\psi_{R,\sigma}(r') + H.C.) \\ H_Q &= \frac{1}{8C}\left(Q_L - Q_R\right)^2, \end{aligned} \tag{A.3}$$

with the charge on each site given by $Q_{L(R)} = e\int d^D r \psi^\dagger_{L(R),\sigma}(r)\psi_{L(R),\sigma}(r)$. It is worth noting that this model assumes that the timescale of the problem is slow compared with the plasma frequency of the electrons in the bulk. This allows for the screening of hole made by an Andreev process electron exiting the bulk so that the interaction between the particle-hole pair does not need to be taken into account.

The partition function of the system is given by $Z = \mathrm{Tr}_{\psi,A}(\exp(-\beta H))$. The Hamiltonian is quartic in ψ_L and ψ_R, but can be decoupled via Hubbard-Stratonovich transformation with two new fields Δ_L and Δ_R which has the general form

$$\exp\left(-\hat{\rho_m} V_{mn} \hat{\rho_n}\right) = \int D\phi \exp\left(-\frac{1}{4}\phi_m V^{-1} \phi_n - i\phi_m \rho_n\right). \tag{A.4}$$

Performing this transformation and then integrating over the now quadratic ψ_L and ψ_R fields, along with the substitution $V = -i\left\langle Q_L - Q_R\right\rangle / 2C$ results in

$$Z = \int D^2\Delta_L D^2\Delta_R DV DA e^{-S}, \tag{A.5}$$

where the action is

$$\begin{aligned} S &= -\mathrm{Tr}\,\ln \mathcal{G}^{-1} \\ &+ \frac{1}{g}\int d^D r dt \left(|\Delta_L|^2 + |\Delta_R|^2\right) + \frac{1}{2}\int dt C V^2 + \int dt d^D r \frac{1}{8\pi}\left(h - h_{ext}\right)^2. \end{aligned} \tag{A.6}$$

The matrix $\hat{\mathcal{G}}^{-1}$ is the Green function of the system in Nambu space, and is given by

$$
\begin{aligned}
\mathcal{G}^{-1} &= \begin{pmatrix} \mathcal{G}_L^{-1} & -\hat{\mathrm{T}}\delta(t-t') \\ -\hat{\mathrm{T}}^\dagger\delta(t-t') & \mathcal{G}_R^{-1} \end{pmatrix} \\
\mathcal{G}_{L(R)}^{-1} &= \left(-\frac{\partial}{\partial t} + \left(\frac{(\nabla - ie\mathbf{A}\sigma_3)^2}{2m} + \mu(\mp)\frac{ie}{2}V \right)\sigma_3 - \hat{\Delta}_{L(R)} \right)\delta(x-x')\delta(t-t') \\
\hat{\Delta}_{L(R)} &= \begin{pmatrix} 0 & \Delta_{L(R)} \\ \Delta^\star_{L(R)} & 0 \end{pmatrix} \\
\hat{\mathrm{T}} &= \begin{pmatrix} \mathrm{T} & 0 \\ 0 & -\mathrm{T}^\star \end{pmatrix}.
\end{aligned}
\tag{A.7}
$$

The superconducting order parameter $\hat{\Delta}_{L(R)}$ may be written explicitly in its real and imaginary parts, $\hat{\Delta}_{L(R)} = \left|\Delta_{L(R)}\right| \exp(-i\phi_{L(R)}\sigma_3)\sigma_1$. If a gauge transformation $U_{L(R)} = \exp(i\phi_{L(R)}\sigma_3/2)$ where $\nabla \cdot A = 0$ is made to make $\Delta_{L(R)}$ real, the Green function of the system takes the form

$$
\begin{aligned}
\mathcal{G}_L^{-1} &= U\mathcal{G}_L^{-1}U^{-1} \\
&= \left(-\frac{\partial}{\partial t} + iv_L\cdot\nabla + \left(\frac{\nabla^2}{2m} + \mu - \frac{m}{2}v_L^2 + \frac{i}{2}\left(\frac{\partial\phi}{\partial\tau} - 2eV \right) \right)\sigma_3 - |\tilde{\Delta}_L| \right) \\
&\times \ \delta(x-x')\delta(t-t'),
\end{aligned}
\tag{A.8}
$$

and similarly for $\mathcal{G}_L^{-1}$ except for $V \to -V$ where the superfluid velocity $v_{L(R)} = -\frac{1}{2m}\left(\nabla\phi_{L(R)} \mp 2e\mathbf{A}\right)$.

All of this just amounts to a rewriting of the the partition function in such a way so that the dependence on $\left|\Delta_{L(R)}\right|$, $\mathbf{A}$, V and $\phi_{L(R)}(\tau)$ has been made explicit. It can be shown that the fluctuations of $\left|\Delta_{L(R)}\right|$, $\mathbf{A}$, and V are strongly suppressed [98, 23] in the deep superconducting regime and the only dynamical degree of freedom is the phase difference $\phi(\tau) = \phi_L(\tau) - \phi_R(\tau)$. If the action is then expanded about $\partial_\tau\phi_{L(R)} \mp 2eV_{L(R)}$ then the first non zero contribution second order (since the first order term is the evaluates to zero as the semi-classical Josephson effect). The resulting action is thus, up to a constant factor

$$
Z \sim \int D\phi \exp\left[-S_T(\phi) - \int d\tau \frac{C}{8e^2}\left(\frac{\partial\phi}{\partial\tau} \right)^2 \right].
\tag{A.9}
$$

The tunneling action S_T in then expanded in the tunneling matrix elements to second order, giving

$$S_T(\phi) = -\int d\tau d\tau' \left[\alpha(\tau-\tau')\cos\frac{\phi(\tau)-\phi(\tau')}{2}) - \beta(\tau-\tau')\cos\frac{\phi(\tau)+\phi(\tau')}{2}\right], \tag{A.10}$$

where the tunneling kernels $\alpha(\tau)$ and $\beta(\tau)$ are

$$\begin{pmatrix}\alpha(\tau)\\ \beta(\tau)\end{pmatrix} = -2\int \frac{d^Dk}{(2\pi)^D}\frac{d^Dk'}{(2\pi)^D}\left|\mathrm{T}(k,k')\right|^2 \begin{pmatrix}G_L(k,\tau)G_R(k',-\tau)\\ F_L(k,\tau)F_R(k',-\tau)\end{pmatrix}. \tag{A.11}$$

Here, G and F are the diagonal and off-diagonal terms in the Nambu-space Green function, the inverse of which is given by Eq. A.7). They are,

$$\begin{aligned} G(k,i\omega_n) &= \frac{i\omega_n+\xi_k}{\omega_n^2+\xi_k^2+\Delta_k^2} \\ F(k,i\omega_n) &= \frac{\Delta_k}{\omega_n^2+\xi_k^2+\Delta_k^2}, \end{aligned} \tag{A.12}$$

where ξ_k is the bare energy measured from the Fermi surface, $\xi_k = k^2/2m - \mu$.

Appendix B

Cluster Expansion Of Josephson Junction Array Effective Action

The effective action for the Josephson junction array system is

$$S = S_C - \sum_{\langle i,j \rangle} \int d\tau \int d\tau' (\alpha(\tau - \tau') \cos(\phi_{ij}(\tau) - \phi_{ij}(\tau')) + \beta(\tau - \tau') \cos(\phi_{ij}(\tau) + \phi_{ij}(\tau'))) \tag{B.1}$$

where S_C consists of one of more charging terms. If the capacitance matrix is non-zero for just the on-site and nearest-neighbor terms, then

$$S_C = \int d\tau \frac{1}{2} \left[\sum_i C_{ii} \left(\frac{\partial \phi_i(\tau)}{\partial \tau} \right)^2 + \sum_{\langle i,j \rangle} C_{ij} \left(\frac{\partial \phi_{ij}(\tau)}{\partial \tau} \right)^2 \right]. \tag{B.2}$$

In order transform this action into a form that is more amenable to analysis, a new field $\psi_i(\tau) = \exp(-i\phi_i(\tau))$ is introduced so that the tunneling action S_T now reads

$$S_T = -\sum_{\langle i,j \rangle} \int d\tau \int d\tau' \, (\, \psi_i \psi_j^\dagger \quad \psi_i^\dagger \psi_j \,)_\tau \begin{pmatrix} \alpha & \beta \\ \beta & \alpha \end{pmatrix}_{\tau - \tau'} \begin{pmatrix} \psi_i^\dagger \psi_j \\ \psi_i \psi_j^\dagger \end{pmatrix}_{\tau'}. \tag{B.3}$$

In a similar manner to [82], the so-called Spherical Approximation is used, whereby the new field ψ_i is subject to the additional constraint $\sum_i |\psi_i(\tau)|^2 = N$. These constraints may be enforced in the partition function by inserting the unity operator, expressed as

$$1 = \int D\psi \left[\delta(\sum_i |\psi_i(\tau)|^2 - N) \prod_i \delta(\psi_i(\tau) - \exp(-i\phi_i(\tau)) \right]. \tag{B.4}$$

The functional form of the delta function is [83]

$$\delta(f(\tau)) = \int_{-\infty}^{\infty} \frac{D\lambda}{2\pi} \exp\left[i \int_0^\beta d\tau \lambda(\tau) f(\tau) \right]. \tag{B.5}$$

Inserting this constraint into the partition function,

$$Z = \int D\psi \delta \left(\sum_i |\psi_i(\tau)|^2 - N \right) \exp\left[-S_T \right]$$
$$\times \int D\phi \int D\boldsymbol{\mu} \exp\left[i \sum_i \int_0^\beta d\tau \left(\boldsymbol{\mu}_i^\dagger(\tau) \cdot \boldsymbol{\psi}_i(\tau) - \boldsymbol{\mu}_i^\dagger \cdot \mathbf{S}(\phi_i(\tau)) \right) - S_C(\phi_i(\tau)) \right] \tag{B.6}$$

where

$$\begin{aligned} \boldsymbol{\mu}_i(\tau) &= \begin{pmatrix} \lambda_i(\tau) \\ i\lambda_i(\tau) \end{pmatrix} \\ \boldsymbol{\psi}_i(\tau) &= \begin{pmatrix} \mathrm{Re}(\psi_i(\tau)) \\ \mathrm{Im}(\psi_i(\tau)) \end{pmatrix} \\ \mathbf{S}(\phi_i(\tau)) &= \begin{pmatrix} S_x(\phi_i(\tau)) \\ iS_y(\phi_i(\tau)) \end{pmatrix} = \begin{pmatrix} \cos(\phi_i(\tau)) \\ i\sin(\phi_i(\tau)) \end{pmatrix}. \end{aligned} \tag{B.7}$$

The expression $U(\boldsymbol{\mu})$ is introduced such that

$$\exp[U(\boldsymbol{\mu})] = \int D\phi \exp\left[i \sum_i \int_0^\beta d\tau \left(\boldsymbol{\mu}_i^\dagger(\tau) \cdot \mathbf{S}(\phi_i(\tau)) \right) + S_C(\phi_i(\tau)) \right]. \tag{B.8}$$

In the classical limit, the contributing part of the action is stationary with respect to $\boldsymbol{\mu}$, so

$$\frac{\partial}{\partial \boldsymbol{\mu}_i(\tau)} \left(i\boldsymbol{\mu}_i(\tau) \cdot \boldsymbol{\psi}_i(\tau) - U(\boldsymbol{\mu}) \right) |_{\boldsymbol{\mu} \to \boldsymbol{\mu}_c}. \tag{B.9}$$

If the partition function is expanded around $\boldsymbol{\mu}_c$ then

$$\int D\boldsymbol{\mu} \exp\left[i \sum_i \int d\tau (\boldsymbol{\mu}_i^\dagger(\tau) \cdot \boldsymbol{\psi}_i(\tau)) - U(\boldsymbol{\mu}) \right]$$
$$= \int D\boldsymbol{\mu} \exp\left[i \sum_i \int d\tau (\boldsymbol{\mu}_{ci}^\dagger(\tau) \cdot \boldsymbol{\psi}_i(\tau)) - U(\boldsymbol{\mu}_c) \right]$$
$$\times \exp\left[-\frac{1}{2} \sum_{i,j} \int d\tau \int d\tau' \boldsymbol{\mu}_i^\dagger(\tau) \left(\frac{\partial^2 U(\boldsymbol{\mu})}{\partial \boldsymbol{\mu}_i^\dagger(\tau) \partial \boldsymbol{\mu}_j(\tau')} \right) \boldsymbol{\mu}_j(\tau') \right] \times \cdots \tag{B.10}$$

Taking the second derivative of B.8 results in

$$\frac{\partial^2 U(\boldsymbol{\mu})}{\partial \boldsymbol{\mu}_i^\dagger(\tau)\partial \boldsymbol{\mu}_j(\tau')} = \left\langle \mathbf{S}(\phi_i(\tau))\mathbf{S}^\dagger(\phi_j(\tau'))\right\rangle - \left\langle \mathbf{S}(\phi_i(\tau))\right\rangle \left\langle \mathbf{S}^\dagger(\phi_j(\tau'))\right\rangle \tag{B.11}$$

where the averages are taken over S_C. The second term evaluates to zero, so that $W(\tau,\tau')_{i,j} = \frac{\partial^2 U(\boldsymbol{\mu})}{\partial \boldsymbol{\mu}_i^\dagger(\tau)\partial \boldsymbol{\mu}_j(\tau')}$ is given explicitly by

$$W(\tau,\tau')_{i,j} = \int D\phi \exp\left[i(\phi_i(\tau) - \phi_j(\tau'))\right] \exp^{-S_C}. \tag{B.12}$$

To solve this integral, introduce the Fourier Transform of $\phi_i(\tau)$ so that the integral becomes

$$W = \int D\phi \prod_{k,n} \exp\left[\frac{i}{\sqrt{N\beta}}\left(e^{-i(\omega_n\tau - kr_i)} - e^{-i(\omega_n\tau' - kr_j)}\right)\phi_{kn} + |\omega_n|^2 C(k)\phi_{kn}^2\right], \tag{B.13}$$

where C(k) is the Fourier transform of an as-yet unspecified capacitance matrix $C_{i,j}$. The integral is now a Gaussian integral of the form

$$\int D\phi \exp[-\frac{1}{2}\phi A\phi + \phi j] = \mathrm{Det}A^{-\frac{1}{2}} \exp\left[\frac{1}{2} j^\dagger A^{-1} j\right]. \tag{B.14}$$

The $\mathrm{Det}A^{-\frac{1}{2}}$ term is an irrelevant normalization term that is ultimately canceled out by the denominator of any average that would be computed. The remaining term gives

$$W = \exp\left[-\frac{1}{2N\beta}\sum_{k,n} \frac{(2 - \exp\left[-i\omega_n(\tau-\tau')\right]\exp\left[-ik(r_i - r_j)\right] + \text{H.C.})}{2\omega_n^2 C(k)}\right]. \tag{B.15}$$

The sum over n diverges unless $r_i = r_j$, so the sum over k may be separated out and may be identified as the effective Coulomb energy E_C whose expression in the continuum limit is

$$E_C = \int \frac{d^D k}{2(2\pi)^{D+1} C(k)}, \tag{B.16}$$

E_C is generally proportional to the inverse capacitance $C(k)$, which will converge under the reasonable condition that the spatial capacitance $C_{i,j}$ between grains i and j

decreases with increasing separation $|r_i - r_j|$. The remaining sum over n is evaluated in the continuum limit, resulting in

$$W(|\tau - \tau'|)_{i,j} = \delta_{ij} e^{-E_C|\tau-\tau'|}. \tag{B.17}$$

This expression, and the entire preceding analysis has been carried out with the implicit assumption that the model is in the $T \to 0$ regime. However for finite T the winding numbers of the phase ϕ_i must be taken into account. The result of the inclusion of these winding numbers amounts to the substitution $\tau -> \tau + T\tau^2$, thereby making the Green function periodic over $[0, \beta]$, as is required formally. Also useful is the zero temperature frequency space representation of this expression which is

$$W(\omega_n) = \frac{\delta_{ij}}{E_C + \omega^2/E_C}. \tag{B.18}$$

With this result in hand, the partition function for the Josephson junction is now

$$Z = \int D\psi \delta \left(\sum_i |\psi_i(\tau)|^2 - N \right) \exp\left[-S_T\right]$$
$$\times \int D\boldsymbol{\mu} \exp\left[i \sum_i \int_0^\beta d\tau \left(\boldsymbol{\mu}_i^\dagger(\tau) \cdot \boldsymbol{\psi}_i(\tau) - \frac{1}{2} \boldsymbol{\mu}_i^\dagger W_{i,j}(|\tau - \tau'|) \boldsymbol{\mu}_j \right) \right]. \tag{B.19}$$

This integral is now Gaussian in $\boldsymbol{\mu}$ so it may be integrated out. The normalization term may be ignored and writing the spherical constraint term as a delta functional, the partition function becomes

$$Z = \int D\psi D\lambda \exp\left[-S_T - \sum_i \int d\tau \psi_i^\dagger(\tau) \left(\frac{W_{i,i}^{-1}(|\tau - \tau'|)}{2} - \lambda_i(\tau) \delta(\tau - \tau') \psi_j(\tau') \right) \right] \tag{B.20}$$

A term proportional to $\int D\lambda \exp\left[i \sum_i \int_0^\beta d\tau \lambda_i(\tau) \right]$ has been left out which does not contribute to the partition function. For $\alpha = \beta = 0$, the frequency domain bare Green function is

$$G_{ij}^{(0)}(\omega_n) = \frac{2\delta_{ij}}{\omega_n^2/E_C + E_C - 2\lambda_i(0)} \tag{B.21}$$

which, under the normalization condition $\int \frac{d\omega}{2\pi} G^{(0)}(\omega) = 1$ fixes $\lambda(\omega = 0) \to 0$, and justifying the neglect of the $\int D\lambda \exp\left[i \sum_i \int_0^\beta d\tau \lambda_i(\tau)\right]$ term, because $\lambda(0) = \int d\tau \lambda(\tau)$. This bare green function is used throughout to build the diagrams that will ultimately determine the electrical conductivity of the Josephson array.

Appendix C

Josephson Junction Array Green Functions

If the calculation of the dressed Green function is restricted to include only local and nearest-neighbor first order processes in the self energies, then Eq. 2.1 can be written as the coupled equations

$$\begin{aligned} G_0 &= G_0^{(0)} + G_0^{(0)}\Sigma_0 G_0 + G_0^{(0)}\Delta_0 F_0 \\ G_1 &= G_0^{(0)}\Sigma_1 G_0 + G_0^{(0)}\Delta_1 F_0 + G_0^{(0)}\Sigma_0 G_1 + G_0^{(0)}\Delta_0 F_1 \\ F_0 &= G_0^{(0)}\Delta_0 G_0 + G_0^{(0)}\Sigma_0 F_0 \\ F_1 &= G_0^{(0)}\Delta_1 G_0 + G_0^{(0)}\Sigma_1 F_0 + G_0^{(0)}\Delta_0 G_1 + G_0^{(0)}\Sigma_0 F_1, \end{aligned} \tag{C.1}$$

where the bare single particle Green function is given by $G^{(0)} = 1/(i\omega - E_c)$.

$$\begin{aligned} G_0 &= -\frac{1}{2}(e^{-E_{C+}\tau} + e^{-E_{C-}\tau}\Theta(\tau\ \mathrm{sign}(E_{C-}))\ \mathrm{sign}(E_{C-})) \\ G_1 &= \frac{1}{2}\tau((\Delta_1 + \Sigma_1)e^{-E_{C+}\tau} - (\Delta_1 - \Sigma_1)e^{-E_{C-}\tau}\Theta(\tau\ \mathrm{sign}(E_{C-}))\ \mathrm{sign}(E_{C-})) \\ F_0 &= -\frac{1}{2}(e^{-E_{C+}\tau} - e^{-E_{C-}\tau}\Theta(\tau\ \mathrm{sign}(E_{C-}))\ \mathrm{sign}(E_{C-})) \\ F_1 &= \frac{1}{2}\tau((\Delta_1 + \Sigma_1)e^{-E_{C+}\tau} + (\Delta_1 - \Sigma_1)e^{-(E_{C-})\tau}\Theta(\tau\ \mathrm{sign}(E_{C-}))\ \mathrm{sign}(E_{C-})) \end{aligned} \tag{C.2}$$

where $E_{C+} = E_C + \Delta_0 + \Sigma_0$ and $E_{C-} = E_C - \Delta_0 + \Sigma_0$. E_C is related to the sum of the self and intra-grain capacitances and as such is much larger than the emergent

self energies of the quasiparticle propagators in the vicinity of a phase transition. Therefore sign(E_{C-}) = 1 and also near the emergent phase boundaries $E_{C+} \approx E_C$ and $E_{C-} \approx E_C$. To calculate F_0 it is necessary to expand in powers of Δ_0 prior to making this simplification. The resulting dressed Green functions are

$$\begin{aligned} G_0 &= e^{-E_C\tau} \\ G_1 &= \Sigma_1\tau e^{-E_C\tau} \\ F_0 &= \Delta_0\tau e^{-E_C\tau} \\ F_1 &= \Delta_1\tau e^{-E_C\tau}. \end{aligned} \tag{C.3}$$

Appendix D

Diagram Methods For The Josephson Junction Array

D.1 Interactions

From the Josephson junction array action (Eq. 4.10) it is evident that the dissipation term α which describes the Andreev process, involves the transfer of both a particle and hole from grain i to grain j whereas the Cooper term β describes the transfer of two particles (the Cooper pair) from site i to site j. In terms of the Feynman diagrams this means that each interaction is connected at a vertex to two green functions, and that there is an incoming and outgoing particle from sites i and j. There cannot be a situation where both Green functions at the vertex involve particles entering and exiting from the same site.

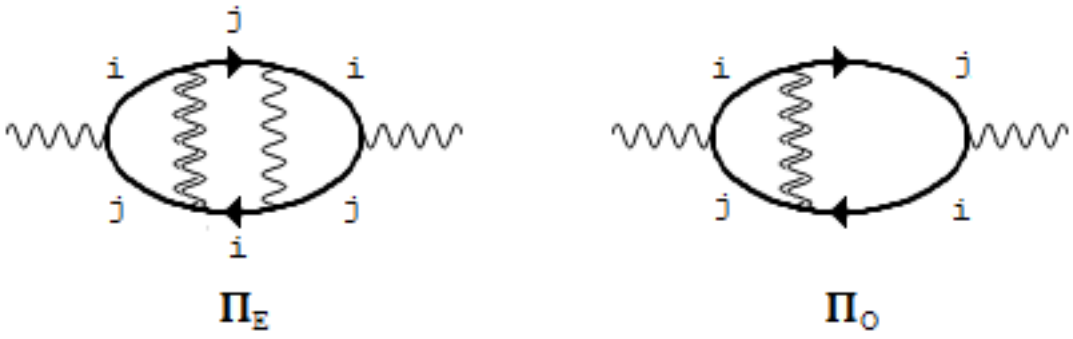

Figure D.1: Even and odd polarization diagrams

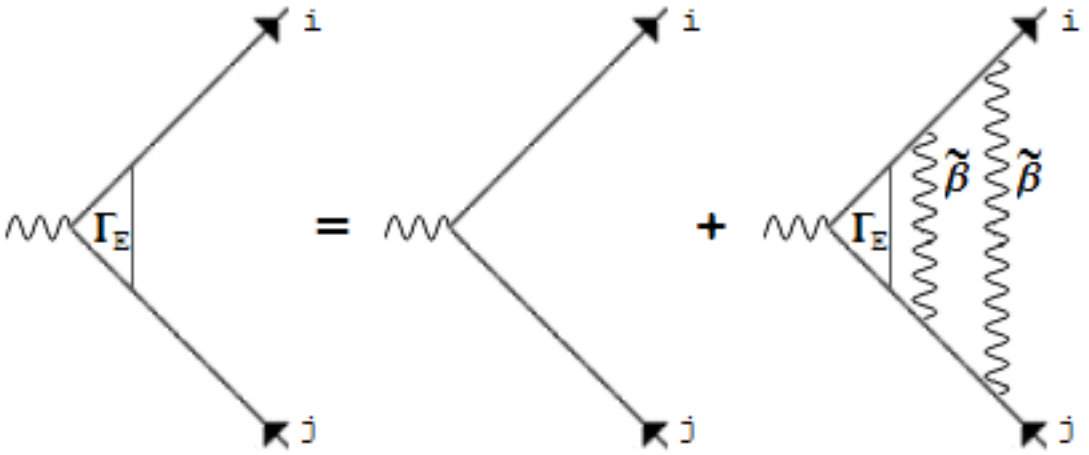

Figure D.2: Even vertex

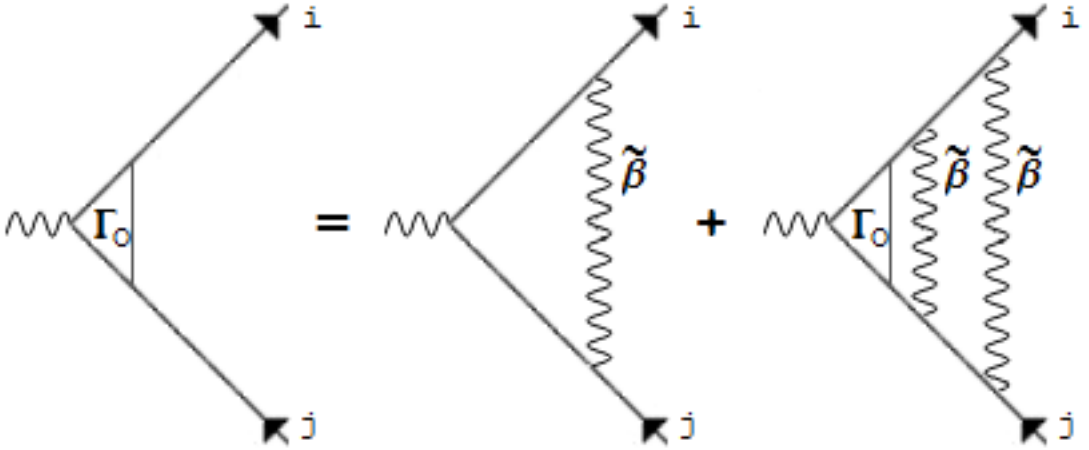

Figure D.3: Odd vertex

This last condition places a constraint on the allowable interaction lines that constitute the Polarization Π. The dominant contribution to Π comes from the terms that have no crossed interaction lines (the ladder diagrams). Since each crossed interaction line places an additional constraint on the frequency integration, the effective phase space over which the integral is evaluated, and hence its magnitude is reduced. Having made this simplification to the types of diagrams being considered, the only allowable interactions are the β lines (Fig. D.1). A distinction can be made depending on whether the number of interactions is even (Π_E) or odd (Π_O), which obey $\Pi = \Pi_E + \Pi_O$.

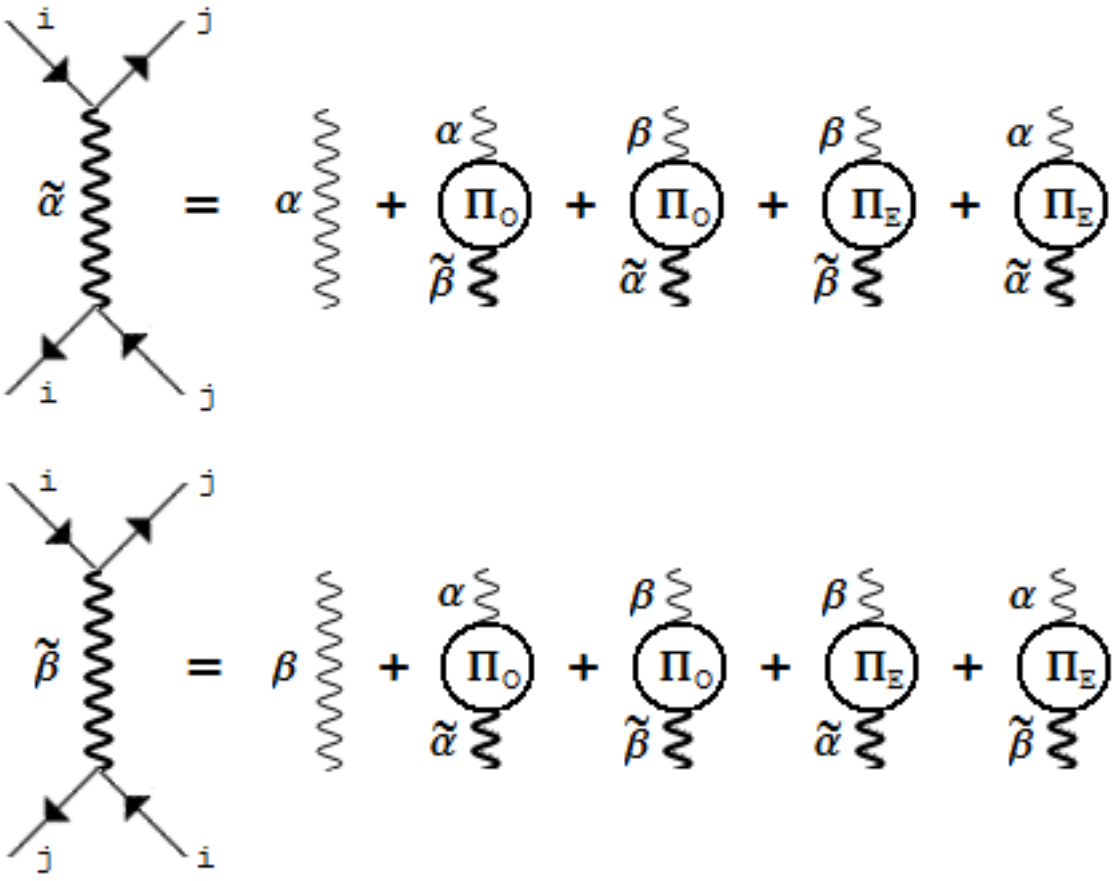

Figure D.4: The first order contributions to $\tilde{\alpha}$ and $\tilde{\beta}$

The same distinction can be made for the vertex operator Γ, splitting the contribution to Γ into constituent parts involving even and odd numbers of non-crossing β lines so that $\Gamma = \Gamma_E + \Gamma_O$. A self-consistent equation may be written for Γ_E and Γ_O according to the diagrams in Fig. D.2 and D.3 respectively. This allows the computation of the vertex and related polarization operators. The vertex diagrams carry a contribution proportional to $\tilde{\beta}^N$ where N is the number of interaction lines, resulting in the following for Π and Γ

$$\begin{aligned} \Gamma_E = \Pi_E &= \frac{1}{1-\tilde{\beta}^2} \\ \Gamma_O = \Pi_O &= \frac{\tilde{\beta}}{1-\tilde{\beta}^2} \end{aligned} \tag{D.1}$$

The dressed interactions $\tilde{\alpha}$ and $\tilde{\beta}$ may be written in terms of bare interactions α

and β along with the polarizations Π_E and Π_O in a self consistent manner as shown in Fig. D.4. These diagrams yield the following equations for α and β

$$\begin{aligned}\tilde{\alpha} &= \alpha + (\alpha\tilde{\beta} + \beta\tilde{\alpha})\Pi_O + (\alpha\tilde{\alpha} + \beta\tilde{\beta})\Pi_E \\ \tilde{\beta} &= \beta + (\alpha\tilde{\alpha} + \beta\tilde{\beta})\Pi_O + (\alpha\tilde{\beta} + \beta\tilde{\alpha})\Pi_E. \end{aligned} \tag{D.2}$$

The solution to these coupled equations is

$$\begin{aligned}\tilde{\alpha} &= \frac{(1-\alpha)(\alpha+\beta^2)}{(1-\alpha)^2 - 4\beta^2} \\ \tilde{\beta} &= \frac{\beta + \alpha^2\beta - 2\beta^2}{(1-\alpha)^2 - 4\beta^2}, \end{aligned} \tag{D.3}$$

which for $\beta \to 0$ results in the rescaling of $\tilde{\alpha} = \frac{\alpha}{1+\alpha}$ typical of granular metals [99].

D.2 Self Energy

The ultimate goal of this exercise is to generate equations for the standard and anomalous local and nearest neighbor self energies Σ_0, Σ_1, Δ_0 and Δ_1. As with the calculation of the Polarization operators, it is assumed that the largest contribution to these terms comes from diagrams that contain only non-crossing interaction lines. In this case, the self energies are a self-consistent series of ladder diagrams, with the exception of the non-local self energy Σ_1 which also has Hartree contributions (Fig. D.5).

In these diagrams, it is assumed that each interaction line is also accompanied by any vertices (even or odd) that may be inserted while maintaining the overall validity of the diagram. Also, the Green functions appearing in the diagrams are $G^{(0)}_{i,j}$ which is only non-zero for $i = j$. The expansions for Σ_0 and Δ_0 are multiplied by a factor of the coordination number z, which is the number of nearest neighbors in the lattice. In the equations for Σ_0, and Δ_0 the particle may jump to any neighboring grain, whereas in the diagrams for Σ_1 and Δ_1 the grains on which these interactions take place are fixed explicitly by the choice of i and j. With the vertex contributions included the diagrams in Fig. D.5 result in the Eq. 2.1 which, in the $\omega \to 0$ limit become

$$\lim_{\omega\to 0}\Sigma_0(\omega) = z\lim_{\omega\to 0}(1+\Sigma_0(\omega))\left(\Gamma_E^2\tilde{\beta} + 2\Gamma_E\Gamma_O\tilde{\alpha} + \Gamma_O^2\tilde{\beta}\right)$$

$$
\begin{aligned}
\lim_{\omega\to 0}\Sigma_1(\omega) &= \lim_{\omega\to 0}\Sigma_1(\omega)\left(\Gamma_E^2+\Gamma_O^2\right)\left(2\tilde{\beta}+\tilde{\alpha}\right)+2\Gamma_E\Gamma_O\left(2\tilde{\alpha}+\tilde{\beta}\right)\\
\lim_{\omega\to 0}\Delta_0(\omega) &= z\lim_{\omega\to 0}\Delta_0(\omega)\left(\Gamma_E^2\tilde{\beta}+2\Gamma_E\Gamma_O\tilde{\alpha}+\Gamma_O^2\tilde{\beta}\right)\\
\lim_{\omega\to 0}\Delta_1(\omega) &= z\lim_{\omega\to 0}\Delta_(\omega)\left(\Gamma_E^2\tilde{\alpha}+\Gamma_O^2\tilde{\alpha}+2\Gamma_E\Gamma_O\tilde{\beta}\right). \qquad \text{(D.4)}
\end{aligned}
$$

The emergence of $\frac{d\Sigma_0}{d\omega}$, Σ_1, Δ_0, and Δ_1 are presumed to signify boundaries of the electrical conductivity phase diagram for the Josephson junction and are given by the contours

$$
\begin{aligned}
1 &= z\left(\Gamma_E^2\tilde{\beta}+2\Gamma_E\Gamma_O\tilde{\alpha}+\Gamma_O^2\tilde{\beta}\right)\\
1 &= \left(\Gamma_E^2+\Gamma_O^2\right)\left(2\tilde{\beta}+\tilde{\alpha}\right)+2\Gamma_E\Gamma_O\left(2\tilde{\alpha}+\tilde{\beta}\right)\\
1 &= z\left(\Gamma_E^2\tilde{\beta}+2\Gamma_E\Gamma_O\tilde{\alpha}+\Gamma_O^2\tilde{\beta}\right)\\
1 &= z\left(\Gamma_E^2\tilde{\alpha}+\Gamma_O^2\tilde{\alpha}+2\Gamma_E\Gamma_O\tilde{\beta}\right), \qquad \text{(D.5)}
\end{aligned}
$$

where Γ_E and Γ_O are given by D.1 and $\tilde{\alpha}$ and $\tilde{\beta}$ are given by Eq. D.3.

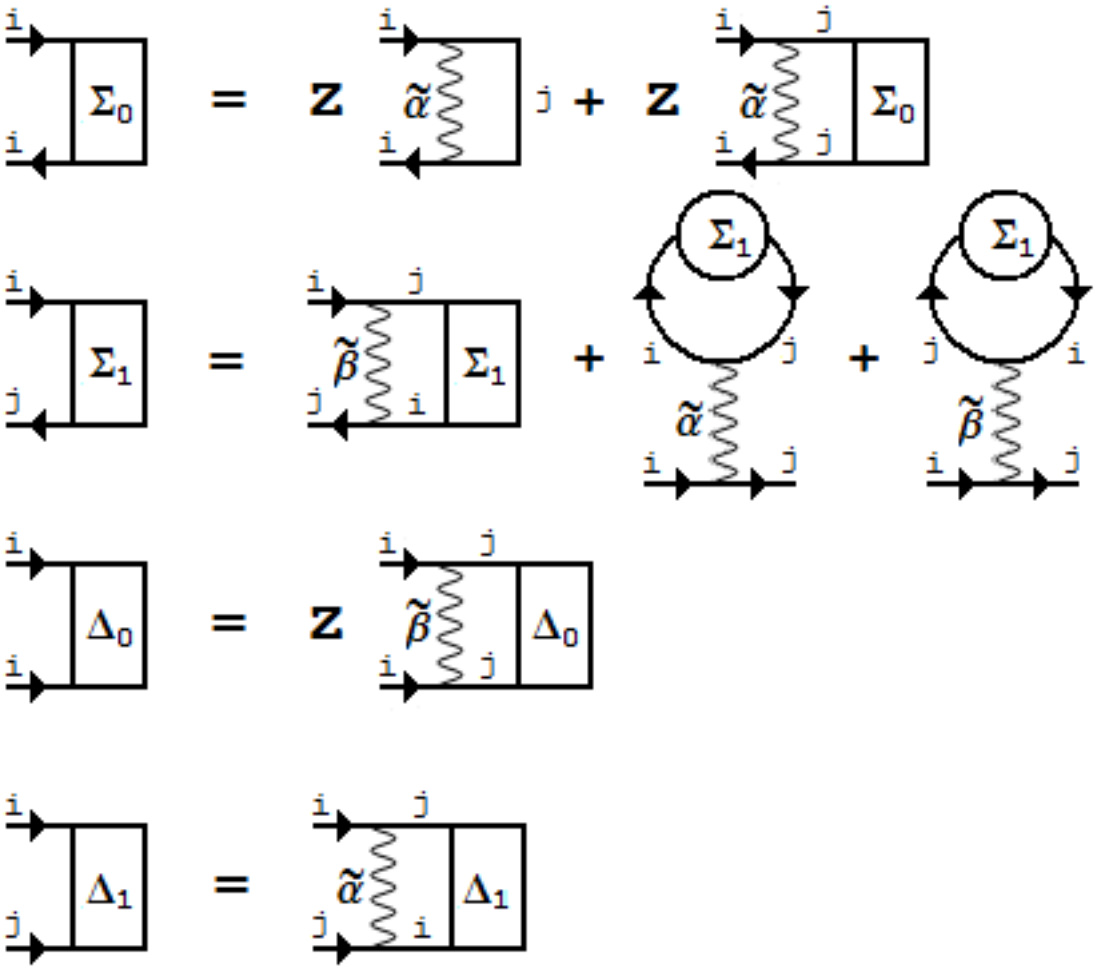

Figure D.5: Order parameter self consistent diagrams

Appendix E

Josephson Junction Array Electrical Conductivity Integrals

To arrive at an expression for the electrical conductivity of the Josephson Junction array, the integrals appearing in Eq. 4.28 must be evaluated. These integrals have the forms

$$\begin{aligned}\sigma_{\mu\mu}(\omega) &\approx \frac{c'}{\omega}\int_0^{1/T} d\tau(\alpha\frac{1-e^{i\Omega_m\tau}}{\tau^2}[G_1^2(0)+G_0^2(\tau)+F_1^2(\tau)] \\ &+ \beta\frac{1+e^{i\Omega_m\tau}}{\tau^2}[G_1^2(0)+G_1^2(\tau)+F_0^2(\tau)]) \end{aligned} \tag{E.1}$$

where the on-site and nearest-neighbor normal and anomalous Green functions $G_0(\tau)$, $G_1(\tau)$, $F_0(\tau)$ and $F_1(\tau)$ are given by Eq. C.3. The above equation is not periodic over $[0, 1/T]$ because it does not take into account the winding numbers of the field $\phi_i(\tau)$. If this correction is made, and the proper periodic forms of $\alpha(\tau)$ and $\beta(\tau)$ are introduced 2.1, then

$$\begin{aligned}\sigma_{\mu\mu}(\omega) &\approx \frac{c}{\omega}\int_0^{1/T} d\tau(\alpha\frac{1-e^{i\Omega_m\tau}}{\sin^2(\pi T\tau)}[G_1^2(0)+G_0^2(\tau-T\tau^2)+F_1^2(\tau-T\tau^2)] \\ &+ \beta\frac{1+e^{i\Omega_m\tau}}{\sin^2(\pi T\tau)}[G_1^2(0)+G_1^2(\tau-T\tau^2)+F_0^2(\tau-T\tau^2)]) \end{aligned} \tag{E.2}$$

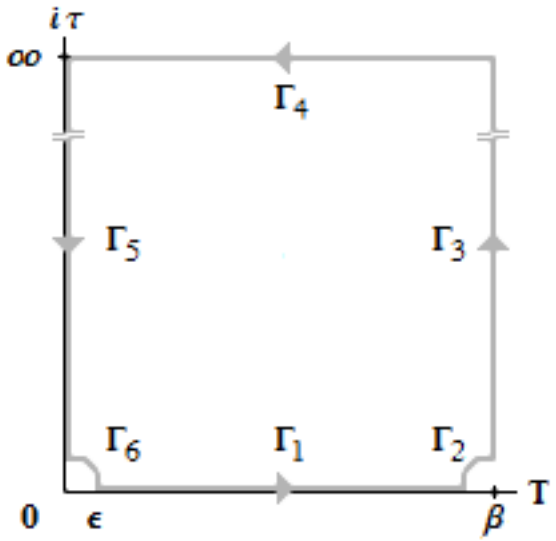

Figure E.1: The contour over which the conductivity integrals are computed

E.1 Integral Involving $G_0^2(\tau)$

The $G_0^2(\tau)$ contribution to the integral in Eq. E.2 does not rely upon the emergence of any of of the self-energies Σ_1, Δ_0 and Δ_1 and is therefore present for all values of $\alpha \neq 0$. These terms should represent the insulating phase of the Josephson Junction array. In performing the computation, it is not possible to perform the analytic continuation from the imaginary-time to a real-time integral simply through the substitution $\tau \to it$ because of the poles at $\{0, 1/T\}$ in the integrand. Therefore the integral is performed over the contour in Fig. E.1. The integrand has no poles inside the contour, so

$$\sigma_{1,\alpha} = \int_{\Gamma_1} = -\int_{\Gamma_2} - \int_{\Gamma_3} - \int_{\Gamma_4} - \int_{\Gamma_5} - \int_{\Gamma_6}. \tag{E.3}$$

The α contribution to this term is

$$\sigma_{1,\alpha} = c\frac{\alpha}{\omega}\int_0^{1/T} d\tau \left.\frac{1-e^{i\Omega_m\tau}}{\sin^2(\pi T\tau)}\right|_{\Omega_m\to -i\omega+0_+} e^{-2E_C(\tau - T\tau^2)}. \tag{E.4}$$

Along Γ_3, it is

$$\int_{\Gamma_3} = c\frac{\alpha}{\omega}\int_\epsilon^\infty idt \left.\frac{1-e^{i\Omega_m(it+1/T)}}{\sin^2(\pi T(it+1/T))}\right|_{\Omega_m\to -i\omega+0_+} e^{-2E_C((it+1/T)-T(it+1/T)^2)}. \tag{E.5}$$

Keeping in mind that Ω_m is a Matsubara frequency $e^{i\Omega_m/T} = 1$, so that this integral now takes the form

$$\int_{\Gamma_3} = -ic\frac{\alpha}{\omega}\int_\epsilon^\infty idt \frac{1-e^{i\omega t}}{\sinh^2(\pi Tt)} e^{-2E_C Tt^2} e^{2iE_C t}. \tag{E.6}$$

In a similar manner the integral over Γ_5 yields

$$\int_{\Gamma_5} = ic\frac{\alpha}{\omega}\int_{\epsilon}^{\infty} idt\frac{1-e^{i\omega t}}{\sinh^2(\pi T t)}e^{-2E_C T t^2}e^{-2iE_C t}. \tag{E.7}$$

So that the combined contribution of the integral over contours Γ_3 and Γ_5 is

$$\int_{\Gamma_3+\Gamma_5} = c\frac{2\alpha}{\omega}\int_{\epsilon}^{\Lambda} dt\frac{1-e^{i\omega t}}{\sinh^2(\pi T t)}e^{-2E_C T t^2}\sin(2E_C t), \tag{E.8}$$

where the upper cutoff Λ has been introduced so that as long as $\omega \ll \Lambda^{-1}$ the integrand may be expanded in ω. The existence of a minimum energy gap Σ_0 which retains a non-zero value for $\omega \to 0$ ensures the existence of this upper bound, so the integral is now

$$\int_{\Gamma_3+\Gamma_5} = -\frac{2ic\alpha}{T^2}e^{\frac{E_C T}{2}\frac{\partial^2}{\partial E_C^2}}\int_{\epsilon}^{\Lambda} dt\frac{t\sin(\frac{2E_C}{T}t)}{\sinh^2(\pi t)} \tag{E.9}$$

The integrand is well behaved, having a vanishing first derivative at both $t \to 0$ and $t \to \infty$ so the bounds in the above integral go from $[\epsilon, \Lambda] \to [0, \infty]$. This allows us to use the standard table integral

$$\int_0^{\infty} dx\frac{x\sin(ax)}{\sinh^2(\pi x)} = \frac{1}{2\pi}\frac{a-\sinh(a)}{1-\cosh(a)}. \tag{E.10}$$

Employing this identity,

$$\int_{\Gamma_3+\Gamma_5} = -\frac{ic\alpha}{\pi T^2}e^{\frac{E_C T}{2}\frac{\partial^2}{\partial E_C^2}}\left(\frac{2E_C/T-\sinh(2E_C/T)}{1-\cosh(2E_C/T)}\right). \tag{E.11}$$

As for the other contours, the integral along Γ_4 vanishes, however both Γ_2 and Γ_6 do provide a contribution. The integrand attains a constant value at the poles $\{0, 1/T\}$ so that

$$\int_{\Gamma_2} + \int_{\Gamma_6} = -\frac{c\alpha}{\pi^2 T^2}\int_{\Gamma_2}\frac{d\tau}{1/T-\tau} - \frac{c\alpha}{\pi^2 T^2}\int_{\Gamma_6}\frac{d\tau}{\tau} \tag{E.12}$$

which, with the substitution $\tau = \epsilon e^{i\theta}$ this integral becomes

$$\frac{-ic\alpha}{\pi^2 T^2}\int_{\pi}^{0} d\theta = \frac{ic\alpha}{\pi T^2}. \tag{E.13}$$

The total conductivity of the insulating phase due to α is

$$\sigma_{1,\alpha} = -\frac{ic\alpha}{\pi T^2}e^{\frac{E_C T}{2}\frac{\partial^2}{\partial E_C^2}}f(2E_C/T), \tag{E.14}$$

where

$$f(a) = 2\frac{(a-1)e^{-a} + e^{-2a}}{(1-e^{-a})^2}. \tag{E.15}$$

If this result is expanded for $T \ll E_C$ then with $c = \frac{i\pi}{2}T^2$

$$\sigma_{1,\alpha} = \alpha\frac{E_C}{T}e^{-2E_C/T}. \tag{E.16}$$

E.2 Integrals Involving $G_1^2(0)$

Both the α and β terms have contributions of this type, but the resulting conductivity is quite different for each case. They will be treated separately.

E.2.1 α Term

$$\sigma_{2,\alpha} = \frac{c\alpha}{\omega}\int_0^{1/T} d\tau \frac{1-e^{i\Omega_m\tau}}{\sin^2(\pi T\tau)}G_1^2(0) \tag{E.17}$$

The only value of τ that results in a contribution to this integral is when $\tau = 1/T$ since $\frac{G_1^2(0)}{\sin^2(\pi T\tau)}$ behaves like a delta function. Writing this as a integration with proper normalization factors inserted,

$$\sigma_{2,\alpha} = \frac{\Sigma_1^2}{E_C^2}\frac{c\alpha}{\omega}\int_0^{1/T} d\tau\ (1-e^{i\Omega_m\tau})\frac{2\pi T\delta(\tau - 1/T)}{\pi^2T^2} \tag{E.18}$$

which gives, under the analytic continuation $\tau \to it$ and $\Omega_m \to i\omega$

$$\sigma_{2,\alpha} = 2\alpha\frac{\Sigma_1^2}{E_C^2}. \tag{E.19}$$

E.2.2 β Term

$$\sigma_{2,\beta} = \frac{\Sigma_1^2}{E_C^2}\frac{c\beta}{\omega}\int_0^{1/T} d\tau \frac{1+e^{i\Omega_m\tau}}{\sin^2(\pi T\tau)}G_1^2(0) \tag{E.20}$$

In the D.C. limit, this integral is dominated by the $1/\omega$ terms, of which there are two non-zero contributions in the sum over τ. Both $\tau = 0$ and $\tau = 1/T$ contribute to the

sum while all other τ have their contributions canceled by $G_1^2(0)$. So using normalization for the δ-function similar to the α case, this contribution to the conductivity gives

$$\sigma_{2,\beta}(0) = 4\beta\frac{T}{\omega}\frac{\Sigma_1^2}{E_C^2} \tag{E.21}$$

E.3 Integrals Involving $G_1^2(\tau)$, $F_0^2(\tau)$, or $F_1^2(\tau)$

E.3.1 α Term

This integral has the form

$$\sigma_{3,\alpha} = \frac{c\alpha}{\omega}\int_0^{1/T} d\tau \frac{1-e^{i\Omega_m\tau}}{\sin^2(\pi T\tau)}F_1^2(\tau) \tag{E.22}$$

Since $F_1(\tau) = -\Sigma_1\frac{\partial}{\partial E_C}G_0(\tau)$ it is possible to cast this integral in the form

$$\sigma_{3,\alpha} = \frac{c\alpha}{4\omega}\frac{\partial^2}{\partial E_C^2}\int_0^{1/T} d\tau \frac{1-e^{i\Omega_m\tau}}{\sin^2(\pi T\tau)}G_0^2(\tau), \tag{E.23}$$

from which the contribution to the conductivity is determined to be

$$\sigma_{3,\alpha} = \alpha\frac{2\Delta_1^2(E_C-T)e^{-2E_C/T}}{T^3}. \tag{E.24}$$

This result carries with it the range of validity from the previous expressions that it is based on, so this contribution to the conductivity is only valid for $T \ll E_C$ and $\Delta_1 \ll E_C$.

E.3.2 β Term

There are two terms, the $G_1^2(\tau)$ and $F_0^2(\tau)$, that provide a contribution to the β part of the conductivity. Apart from their different constants they carry with them, Σ_1 and Δ_0 respectively, they are handled in an identical manner. This integration is performed in a similar manner to the $\sigma_{1,\alpha}$ term by integrating around the contour in Fig. E.1. The following is the computation of the Σ_1 contribution.

$$\sigma_{3,\beta} = \frac{c\beta}{\omega}\int_0^{1/T} d\tau \frac{1+e^{i\Omega_m\tau}}{\sin^2(\pi T\tau)}G_1^2(\tau) \tag{E.25}$$

The integrals over contours Γ_3 and Γ_5 may be summed to get

$$\begin{aligned}\int_{\Gamma_3}+\int_{\Gamma_5} &= -\frac{ic\beta\Sigma_1^2}{\omega}\int_\epsilon^\infty dt\frac{1+e^{i\omega t}}{\sinh^2(\pi Tt)}e^{-2E_CTt^2}\times \\ &\times\ 2i((t^4T^2-t^2)\sin(2E_Ct)-2t^3T\cos(2E_Ct)).\end{aligned} \tag{E.26}$$

In the D.C. limit, the real part of this expression is

$$\mathrm{Re}\int_{\Gamma_3}+\int_{\Gamma_5} = -\pi\beta\Sigma_1^2 e^{\frac{E_CT}{2}\frac{\partial^2}{\partial E_C^2}}\left(\frac{T^2}{8}\frac{\partial^4}{\partial E_C^4}+\frac{T}{2}\frac{\partial^3}{\partial E_C^3}+\frac{1}{2}\frac{\partial^2}{\partial E_C^2}\right)\int_\epsilon^\infty dt\frac{t\sin(\frac{2E_C}{T}t)}{\sinh^2(\pi t)}. \tag{E.27}$$

This expression can be evaluated using the integral in Eq. E.10. While it is a complicated expression, it just describes the same insulating behavior exhibited already by $\sigma_{\alpha,1}$ so the inclusion of this term produces nothing more than an additional (small) contribution to the insulator conductivity proportional to Σ_1^2 or Δ_0^2. The integral over contours Γ_2 and Γ_6 contribute more substantially. Expanding the integral around $\tau=0$ and integrating over these contours,

$$\int_{\Gamma_2}+\int_{\Gamma_6}=\frac{2c\beta}{\pi^2T^2\omega}\int_{\Gamma_2+\Gamma_6}d\tau \tag{E.28}$$

Which, after letting $\tau\to it\to i\epsilon e^{i\theta}$ and integrating gives $\sigma_{3,\beta}=\frac{4\epsilon}{\pi\omega}\beta$, where since epsilon is small but finite $\frac{\epsilon}{2\pi\omega}$ is identified as a delta function. Therefore the conductivity from these terms is

$$\sigma_{3,\beta}=2\beta\delta(\omega)(\frac{\Sigma_1^2}{E_C^2}+\frac{\Delta_1^2}{E_C^2}). \tag{E.29}$$

Finally to compute the longitudinal conductivity (Eq. 4.29) all these contributions are added so that $\sigma_{\mu\mu}=\sigma_{\alpha,1}+\sigma_{\alpha,2}+\sigma_{\alpha,3}+\sigma_{\beta,2}+\sigma_{\beta,3}$.

REFERENCES

[1] J. S. Bell, *Speakable and Unspeakable in Quantum Mechanics* (Cambridge University Press, 1987).

[2] A. Einstein, B. Podolsky, and N. Rosen, Phys. Rev. **47**, 777 (1935).

[3] J. S. Bell, Physics **1**, 195 (1964).

[4] S. Sachdev, *Quantum Phase Transitions*, 2nd ed. (Cambridge University Press, 2011).

[5] G. Jaeger, Vol. Quantum Information (Springer Science + Business Media, LLC, 2007).

[6] C. H. Bennett and S. J. Wiesner, Phys. Rev. Lett. **69**, 2881 (1992).

[7] C. H. Bennett, G. Brassard, C. Crepeau, R. Jozsa, A. Peres, and W. K. Wootters, Phys. Rev. Lett. **70**, 1895 (1993).

[8] M. Nielson and I. Chuang, *Quantum Computation and Quantum Communication* (Cambridge University Press, 2000).

[9] D. Bouwmeester, J.-W. Pan, K. Mattle, M. Eibl, H. Weinfurter, and A. Zeilinger, Nature **390**, 575 (1997).

[10] A. Rauschenbeutel, G. Nogues, S. Osnaghi, P. Bertet, M. Brune, J.-M. Raimond, and S. Haroche, Science **288**, 2024 (2000).

[11] M. Bayer, P. Hawrylak, K. Hinzer, S. Fafard, M. Korkusinski, Z. R. Wasilewski, O. Stern, and A. Forchel, Science **291**, 451 (2001).

[12] M. Riebe, M. Haffner, C. F. Roos, W. Hansel, J. Benhelm, G. P. T. Lancaster, T. W. Korber, C. Bechner, F. Schmidt-Kaler, D. F. V. James, and R. Blatt, Nature **429**, 734 (2004).

[13] V.Bouchiat, D.Vion, P.Joyez, D. Esteve, and M. Devoret, Phys. Scripta **T76**, 165 (1998).

[14] T. Orlando, J. Mooij, L. Tian, C. H. van der Wal, L. S. Levitov, S. Lloyd, and J. Mazo, Phys. Rev. B. **60**, 398 (1999).

[15] G. Blatter, V. B. Geshkenbein, and L. B. Ioffe, Phys. Rev. B. **63**, 174511 (2001).

[16] H. Bethe, Z. Phys. **76**, 205 (1931).

[17] S. Bose, Phys. Rev. Lett. **91**, 207901 (2003).

[18] V. Subrahmanyam, Phys. Rev. A **69**, 034304 (2004).

[19] T. J. Osborne and N. Linden, Phys. Rev. A **69**, 052315 (2004).

[20] L. C. Venuti, C. D. E. Boschi, and M. Roncaglia, Phys. Rev. Lett. **99**, 060401 (2007).

[21] L. Amico and A. Osterloh, J. Phys. A: Math. Gen. **37**, 291 (2004).

[22] L. Amico, A. Osterloh, F. Plastina, R. Fazio, and G. M. Palma, Phys. Rev. A **69**, 022304 (2004).

[23] G. Schon and A. Zaikin, Phys. Rep. **198**, 237 (1990).

[24] C. Bruder, A. van Otterlo, and G. T. Zimanyi, Phys. Rev. B. **51**, 12904 (1995).

[25] T. S. Barash, V. Galaktionov, and A. Zaikin, Phys. Rev. B. **52**, 665 (1995).

[26] M. H. S. Amin and A. Y. Smirnov, Phys. Rev. Lett. **92**, 017001 (2004).

[27] Y. V. Fominov, A. A. Golubov, and M. Y. Kupriyanov, JETP Lett. **77**, 587 (2003).

[28] Y. N. Joglekar, A. H. Neto, and A. V. Balatsky, Phys. Rev. Lett. **92**, 037004 (2004).

[29] Y. N. Joglekar, A. H. Neto, and A. V. Balatsky, Phys. Rev. Lett. **94**, 219901 (2005).

[30] D. V. Khveshchenko, Phys. Rev. Lett. **96**, 027004 (2006).

[31] A. Aspect, P. Grangier, and G. Roger, Phys. Rev. Lett. **47**, 460 (1981).

[32] L. Amico, R. Fazio, A. Osterloh, and V. Vedral, Rev. Mod. Phys. **80**, 517 (2008).

[33] C. H. Bennett, D. P. DiVincenzo, J. A. Smolin, and W. K. Wootters, Phys. Rev. A **54**, 3824 (1996).

[34] M. B. Plenio and V. Vedral, Contemp. Phys. **39**, 431 (1998).

[35] V. Coffman, J. Kundu, and W. K. Wootters, Phys. Rev. A **61**, 052306 (2000).

[36] D. Brub, J. Math. Phys. **43**, 4237 (2002).

[37] V. Vedral, M. B. Plenio, M. A. Rippin, and P. L. Knight, Phys. Rev. Lett. **78**, 2275 (1997).

[38] W. K. Wootters, Phys. Rev. Lett. **80**, 2245 (1998).

[39] C. H. Bennett, H. J. Bernstein, S. Popescu, and B. Schumacher, Phys. Rev. A **53**, 2046 (1996).

[40] S. Hill and W. K. Wootters, Phys. Rev. Lett. **78**, 5022 (1997).

[41] S. Bandyopadhyay, G. Brassard, S. Kimmel, and W. K. Wootters, Phys. Rev. A **80**, 012313 (2009).

[42] D. Burgarth and S. Bose, Phys. Rev. A **71**, 052315 (2005).

[43] D. Poilblanc, Phys. Rev. Lett. **105**, 077202 (2010).

[44] A. M. Lauchli and J. Schliemann, Phys. Rev. B. **85**, 054403 (2012).

[45] Z. Weihong, R. H. McKenzie, and R. R. O. Singh, Phys. Rev. B. **59**, 14367 (1999).

[46] V. Mukherjee, U. Divakaran, A. Dutta, and D. Sen, Phys. Rev. B. **76**, 174303 (2007).

[47] J. Hide, W. Son, I. Lawrie, and V. Vedral, Phys. Rev. A **76**, 022319 (2007).

[48] R. H. Crooks and D. Khveshchenko, Phys. Rev. A **77**, 062305 (2008).

[49] N. Meshkov, A. Glick, and H. Lipkin, Nucl. Phys. , 199 (1965).

[50] N. Meshkov, H. Lipkin, and A. Glick, Nucl. Phys. , 211 (1965).

[51] H. Lipkin, N. Meshkov, and A. Glick, Nucl. Phys. , 188 (1965).

[52] H. Diep, *Frustrated Spin Systems* (World Scientific, Singapore, 2005).

[53] H. Mikeska, Chaos, Solitons, Fractals **5**, 2585 (1995).

[54] F. Essler, H. Frahm, F. Gohmann, A. Klumper, and V. Korepin, *The One-Dimensional Hubbard Model* (Cambridge University Press, 2004).

[55] U. Weiss, *Quantum Dissipative Systems* (World Scientific, Singapore, 1999).

[56] M. Cramer and J. Eisert, M. Cramer and J. Eisert **8**, 71 (2006).

[57] E. Lieb, T. Schultz, and D. Mattix, Ann. of Phys. **16**, 407 (1961).

[58] T. Niemeijer, Physica **36**, 377 (1967).

[59] T. Niemeijer, Physica **39**, 313 (1968).

[60] E. Barouch, B. M. McCoy, and M. Dresden, Phys. Rev. A **2**, 1075 (1970).

[61] E. Barouch and B. M. McCoy, Phys. Rev. A **3**, 786 (1971).

[62] E. Barouch and B. M. McCoy, Phys. Rev. A **3**, 2137 (1971).

[63] B. M. McCoy, E. Barouch, and D. B. Abraham, Phys. Rev. A **4**, 2331 (1971).

[64] T. J. Osborne and M. A. Nielsen, Phys. Rev. A **66**, 032110 (2002).

[65] A. Osterloh, L. Amico, G. Falci, and R. Fazio, Nature **416**, 608 (2002).

[66] G. Vidal, J. I. Latorre, E. Rico, and A. Kitaev, Phys. Rev. Lett. **90**, 227902 (2003).

[67] S. Bose, Contemp. Phys. **48**, 13 (2007).

[68] P. Jordan and E. Wigner, Z. Phys. **47**, 631 (1928).

[69] M. Abromowitz and I. A. Stegun, *Handbook of Mathematical Functions With Formulas, Graphs, and Mathematical Tables* (United States Department of Commerce, 1964).

[70] J. E. Bunder and R. H. McKenzie, Phys. Rev. B. **60**, 344 (1999).

[71] J. Kurmann, H. Thomas, and G. Muller, Physica A **112**, 235 (1982).

[72] G. Muller and R. E. Shrock, Phys. Rev. B. **32**, 5845 (1985).

[73] B. Josephson, Rev. Mod. Phys. **152**, 152 (1966).

[74] A. Caldeira and A. J. Legett, Phys. Rev. Lett. **46**, 211 (1981).

[75] D. V. Khveshchenko and R. Crooks, Phys. Rev. B. **84**, 132502 (2011).

[76] V. Ambegaokar, U. Eckern, and G. Schon, Phys. Rev. Lett. **48**, 1745 (1982).

[77] S. Kawabata, S. Kashiwaya, and Y. A. amd Y. Tanaka, Phys. Rev. B. **70**, 132505 (2004).

[78] S. Kawabata, S. Kashiwaya, Y. Asano, and Y. Tanaka, Phys. Rev. B. **72**, 052506 (052506).

[79] T. Yokoyama, S. Kawabata, T. Kato, and Y. Tanaka, Phys. Rev. B. **76**, 134501 (2007).

[80] T. Kopec and J. V. Jose, Phys. Rev. B **60**, 7473 (1999).

[81] T. Kopec and J. V. Jose, Phys. Rev. Lett. **84**, 749 (2000).

[82] T. Polak and T. Kopec, Phys. Rev. B **72**, 014509 (2005).

[83] A. Altland and B. Simmons, *Condensed Matter Field Theory*, 1st ed. (Cambridge University Press, 2006).

[84] M.-C. Cha, M. P. A. Fisher, S. Girvin, M. Wallin, and A. P. Young, Phys. Rev. B. **44**, 6883 (1991).

[85] A. van Otterlo, K. H. Wagenblast, R. Fazio, and G. Schon, Phys. Rev. B. **48**, 3316 (1993).

[86] R. Fazio and D. Zappala, Phys. Rev. B. **53**, R8883 (1996).

[87] K.-H. Wagenblast, R. Fazio, A. van Otterlo, G. Schon, D. Zappala, and G. T. Zimanyi, Physica B **222**, 336 (1996).

[88] J. Hide, Y. Nakata, and M. Murao, "Entanglement and the interplay between staggered fields and couplings," (2012), arXiv:1201.4251v1.

[89] T. Kibble, J. Phys. A **9**, 1387 (1976).

[90] W. H. Zurek, Nature **317**, 505 (1996).

[91] U. Divakaran and A. D. amd Diptiman Sen, Phys. Rev. B. **81**, 054306 (2010).

[92] Z.-X. Liu, Y. Zhou, and T.-K. Ng, Phys. Rev. B. **82**, 144422 (2010).

[93] Y. Niu, S. B. Chung, C.-H. Hsu, I. Mandal, S. Raghu, and S. Chakravarty, Phys. Rev. B. **85**, 035110 (2012).

[94] J. D. Sau, R. M. Lutchyn, S. Tewari, and S. D. Sarma, Phys. Rev. Lett. **104**, 040502 (2010).

[95] J. Linder, Y. Tanaka, T. Yokoyama, A. Sudbo, and N. Nagaosa, Phys. Rev. Lett. **104**, 067001 (2010).

[96] H. Hilgenkamp and J. Mannhart, Rev. Mod. Phys. **74**, 485 (2002).

[97] V. F. Gantmakher and V. T. Dolgopolov, Phys. Usp. **53**, 1 (2010).

[98] U. Eckern, G. Schon, and V. Ambegaokar, Phys. Rev. B. **30**, 6419 (1984).

[99] I. S. Beloborodov, A. V. Lopatin, V. M. Vinokur, and K. B. Efetov, Rev. Mod. Phys. **79**, 469 (2007).